Report PME-FM-91-1

AD-A237 572

POLYMER DRAG REDUCTION OF A ZERO PRESSURE GRADIENT BOUNDARY LAYER

John E. Koskie and William G. Tiederman
School of Mechanical Engineering
Purdue University
West Lafayette, Indiana 47907

February 1991

Technical Report for Period 01 December 1989 - 30 November 1990

DTIC
ELECTE
JUL 0 2 1991
S
B
D

Prepared for

91-03343

REPORT DOCUMENTATION PAGE		READ INSTRUCTIONS BEFORE COMPLETING FORM
1. REPORT NUMBER PME-FM-91-1	2. GOVT ACCESSION NO.	3. RECIPIENT'S CATALOG NUMBER
4. TITLE (and Subtitle) POLYMER DRAG REDUCTION OF A ZERO PRESSURE GRADIENT BOUNDARY LAYER		5. TYPE OF REPORT & PERIOD COVERED Technical Report for 01 Dec. 1989 through 30 Nov. 1990
		6. PERFORMING ORG. REPORT NUMBER
7. AUTHOR(s) John E. Koskie, William G. Tiederman		8. CONTRACT OR GRANT NUMBER(s) N00014-83K-0183
9. PERFORMING ORGANIZATION NAME AND ADDRESS School of Mechanical Engineering Purdue University West Lafayette, IN 47907		10. PROGRAM ELEMENT, PROJECT, TASK AREA & WORK UNIT NUMBERS 4322-754
11. CONTROLLING OFFICE NAME AND ADDRESS Office of Naval Research 800 North Quincy Street Arlington, VA 22217-5000		12. REPORT DATE February 1991
		13. NUMBER OF PAGES 55
14. MONITORING AGENCY NAME & ADDRESS(if different from Controlling Office)		15. SECURITY CLASS. (of this report)
		15a. DECLASSIFICATION/DOWNGRADING SCHEDULE

16. DISTRIBUTION STATEMENT (of this Report)

APPROVED FOR PUBLIC RELEASE:
DISTRIBUTION UNLIMITED

17. DISTRIBUTION STATEMENT (of the abstract entered in Block 20, if different from Report)

18. SUPPLEMENTARY NOTES

19. KEY WORDS (Continue on reverse side if necessary and identify by block number)

Drag reduction; Turbulent boundary layers, concentration measurements

20. ABSTRACT (Continue on reverse side if necessary and identify by block number)

The objective of this portion of the program was to determine the response of a zero pressure gradient boundary layer to slot injection of drag-reducing polymer solution. Attention was focused on the region far downstream of the injector. Two-component velocity data were acquired with a laser Doppler velocimeter. Mean concentration data were measured using a laser induced fluorescence technique. A 1000 ppm solution of Separan AP-273 was injected into the boundary layer at 1 and 2 times the flow rate of the linear sublayer.

DD FORM 1473   EDITION OF 1 NOV 65 IS OBSOLETE
1 JAN 73
S/N 0102-014-6601 |

Results are based on two-component velocity profiles and concentration profiles at four locations downstream of the slot. These locations correspond to momentum thickness Reynolds numbers of 2478, 2978, 3527 and 3935 in an unmodified Newtonian boundary layer. In dimensionless distance from the slot they vary from 52 to 144 times the boundary layer thickness at the slot and 29000 to 81000 wall units using the unmodified Newtonian inner variables at the slot.

There are two major conclusions from the present data. First, the sum of the viscous shear and Reynolds stresses in polymer drag-reduced boundary layers does not always account for the total shear stress in the inner region of the boundary layer. Some additional stress which is due to the polymer is present. The second conclusion is that the slope of the logarithmic region of the mean velocity profile in a polymer drag-reduced flow may increase over the Newtonian slope. The latter feature may depend on the type of polymer additive.

Table of Contents

1. Introduction

The use of long chain polymers to reduce frictional drag in turbulent flows has been well documented in closed channel flows (see e.g. Virk, 1975). These results suggest that injection of polymer solutions into the boundary layers on the fore and sides of ocean going vessels could result in a significant reduction in viscous drag. However, because drag-reducing polymers have very low molecular diffusivities in water, it is expected that once injected into the boundary layer, the polymer additive will remain in the boundary layer at the aft of the vessel. It is therefore important to understand the behavior of polymer filled boundary layers when they encounter an adverse pressure gradient.

As the first part of a study into the behavior of boundary layers with polymer additives in adverse pressure gradients, a zero pressure gradient boundary layer was drag reduced by injecting polymer solutions through a slot. The objectives of this part of the study were to determine the effect of drag-reducing polymers on the mean velocity statistics of a zero pressure gradient boundary layer, and to determine the shear stress distributions in the boundary layer during drag reduction.

2. Experimental Apparatus and Instrumentation

Experiments were performed using a test section inserted into an existing closed loop water channel shown schematically in Figure 1. The facility has four parallel centrifugal pumps each rated at 90 gpm. Water is pumped into the upstream settling chamber which contains a perforated plate and an open cell foam section. Water enters the test section through a pair of smooth two dimensional contractions. A plastic honeycomb with 3.2 mm (1/8 in) cell size and 25 mm (1 in) streamwise length followed by two 18 mesh screens are located in the inlet of the

test section to remove any large scale vorticity which may occur in the corners of the contraction. The test section is rectangular with three fixed walls and one flexible wall. All velocity and concentration measurements are performed in the boundary layer which forms on the fixed vertical wall opposite the flexible wall. The flexible wall is fixed at its upstream end but can be flexed along the rest of its length to vary the streamwise, freestream pressure gradient. The dimensions of the channel at the inlet are 100 mm in y, the direction normal to the measurement wall, and 200 mm in z, the spanwise direction. The total length of the channel is 2300 mm The flexible wall can move so that the outlet has a maximum total dimension in the y direction of 200 mm. The flexible wall is made of 1.6 mm (1/16 in) acrylic. Its position is controlled by a set rods which are accessible from outside the channel. All fixed walls of the test section are made from 13 mm (1/2 in) polycarbonate sheet. Glass windows are inserted into the top and bottom walls of the channel to allow two-component, laser Doppler velocimetry (LDV) measurements in the channel. These windows are mounted so that one side is flush with the measurement wall, and they extend 100 mm from the measurement wall.

The boundary layer is tripped by a 0.8 mm (1/32 in) diameter brass rod located 197 mm from the inlet. When needed, fluid is injected into the boundary layer through a slot located 331 mm downstream of the inlet. The slot is 2.5 mm wide in the streamwise direction, and it injects fluid at an angle of 25 degrees from the wall. Walker et al. (1986) determined that this geometry produces optimal drag reduction in a two dimensional channel flow with Separan AP-273.

Velocity measurements were performed using a two component LDV system in a forward scatter mode. The system was a two color, four beam system. The beams were configured so that they measure components at 45° from the mean freestream flow direction. An effective shift frequency of 500 KHz was used with both components to eliminate fringe bias. Signal

processing was performed by counter type processors. Data acquisition was controlled by a Masscomp model 5520 computer.

Concentration measurements were performed using a technique developed by Walker & Tiederman (1989a). Fluorescein disodium dye was mixed into the polymer at a concentration of 4 ppm before injection. The channel was dyed to a much lower background concentration, and during the experiments undyed fluid was added as needed so that the background dye concentration remained constant. The dye was fluoresced at the measurement location by the 488 nm beam from an Argon-ion laser which entered the boundary layer normally from the wall on which the boundary layer formed. A linear diode array camera measured the light intensity along this beam at a scan rate which was much higher than the highest frequency in the flow. As a result an essentially instantaneous intensity profile was obtained. This profile was digitized for processing by the computer. When the light intensities were converted to dye concentrations the intensity was integrated along the beam to account for attenuation of the beam.

3. Results: Newtonian Boundary Layers

Newtonian zero pressure gradient boundary layer studies were performed to verify the performance of the facility and to provide a data base to which drag reduced flows can be compared. The effectiveness of the boundary layer trip has been evaluated using the Coles wake parameter, Δu^+_{max}. The wake Δu^+ is defined in the relation:

$$u^+ = \frac{1}{\kappa} ln y^+ + B + \Delta u^+$$

Where the superscript indicates normalization with inner variables. The constants κ and B are the usual log-law constants with values of 0.41 and 5.0 respectively. Coles (1962) recommended

that the wake parameter in a Newtonian zero pressure gradient boundary layer vary as a function of the momentum thickness Reynolds number, Re_θ, along the curve shown in Figure 2. The data of Wieghardt, as reanalyzed by Coles (1968), is also shown because the original was used, in part, to establish the 1962 curve. A number of more recent studies are also shown. Purtell et al. (1981), Murliss et al. (1982) and the 8 m/s case of Erm et al. (1985) follow the trend of Coles' 1962 curve, but are somewhat higher. The 14 m/s data of Erm et al. very closely follows the curve for all Reynolds numbers. The only data which lie distinctly below the curve are those of Shah & Antonia (1989). The reason why these various data follow somewhat different trajectories is not clear. The major conclusion from the plot is that the present data, shown as open circles, is clearly consistent with the data of other investigators. Therefore the present trip is satisfactory.

Figure 3 shows the present Newtonian mean streamwise velocity data for all Reynolds numbers, Re_θ, in the present study. This plot can also be interpreted as showing the dimensionless velocity profile for various streamwise locations in one boundary layer because the Reynolds number is varied by moving the streamwise measurement location while the freestream velocity remains fixed. Also shown is a line representing the standard logarithmic relationship using constants of 0.41 and 5.0 as recommended by Coles (1968). All of the present data agree well with the standard log relation in the region $30 \leq y^+ \leq 300$ except for the lowest Reynolds number of 1358 for which the range is approximately $30 \leq y^+ \leq 200$. The start of the wake region at a smaller value of y^+ for $Re_\theta = 1358$ is a low Reynolds number effect which has been observed by other authors including Purtell et al., Erm et al. and Murliss et al..

Figure 4 compares the present streamwise and normal root mean square velocity fluctuation data normalized by inner variables with other recent data at Reynolds numbers of

approximately 3500. Agreement in the near-wall region, where inner normalization is expected to be correct, is excellent except that u′ for the present data between y^+ of 20 and 50 is slightly higher than that of Purtell et al. (1981) and Erm et al. (1985). Fontaine et al. (1990) have also measured values of u'/u_τ in a water boundary layer using an LDV which are slightly higher than those of Purtell et al. and Erm et al.. This difference may be an indication of limitations on the spatial resolution of the hot wire used in these studies which had a dimensionless length of approximately 20 wall units for Purtell et al. and 30 for Erm et al. These lengths could cause a slightly low rms reading very near the wall. Figure 5 compares the inner normalized Reynolds shear stress of the present study to other studies. Agreement with other data in inner region is very good. The variation of the inner normalized velocity statistics, u'/u_τ, v'/u_τ, and $\overline{uv}/u_\tau^2$, with momentum thickness Reynolds number are shown in the appendix.

4. Results: Drag-Reducing Boundary Layers

The zero pressure gradient boundary layer was drag reduced by injection of 1000 ppm polymer solutions. The polymer additive was Separan AP-273, a polyacrylamide. Two separate injection flow rates were used, $Q_i/Q_s = 1$ and $Q_i/Q_s = 2$, where Q_i is the injected volumetric flow rate and Q_s is the flow rate of the linear sublayer assuming a linear sublayer thickness of $y^+ = 8$. Wall shear stress was determined using the strain rate in the linear sublayer and the shear viscosity of the solution. During the first set of experiments, the translation mechanism was not configured to yield sufficient resolution to make measurements in the sublayer. Therefore, the wall strain rate in the Newtonian flow was determined from velocity measurements in the log region, and the location of the probe volume in the linear region was determined from the measured velocity and this strain rate. Polymer was then injected with the probe volume in the

same location, without any movement of the translation system, and the velocity in the polymer flow at the same physical location was determined. This technique therefore gave directly the ratio of the Newtonian and drag-reduced wall strain rates. In some later experiments a dial gage was attached to the translating mechanism to improve the accuracy of determining the probe location so that the wall strain rate could be calculated directly from two velocity measurements in the linear sublayer. In all cases the shear viscosity of the fluid near the wall was assumed to be the same as that of water. The applicability of this assumption will be discussed later.

4.1 Mean concentration data

The near-wall polymer concentration was measured for both injected flow rates at each streamwise location where velocity measurements were performed. Figure 6 shows the variation of polymer concentration with streamwise distance for both injection flowrates. The local mean concentration is normalized by the injected concentration and the distance normal to the wall is made dimensionless by inner variables assuming that the viscosity is the same as the solvent viscosity. It is not clear whether the use of the solvent viscosity is in fact appropriate for all locations in the drag-reduced flows; however, it provides a consistent basis for normalization. In this plot and in all following figures, the streamwise distance from the injector slot, x, is normalized in two ways: first with the boundary layer thickness of the undisturbed boundary layer near the slot, x/δ_s and second with inner variables using the strain rate of the unmodified boundary layer near the slot and the solvent viscosity, x^+. The region of greatest interest in drag-reducing flows is the region $10 \leq y^+ \leq 100$. McComb & Rabie (1982) and Tiedeman et al. (1985) have shown that polymer must be present in this region for drag reduction to occur. It is immediately apparent that the polymer concentration in the region $10 \leq y^+ \leq 100$ decreases as the flow moves downstream and the polymer mixes farther out into the boundary layer. This

process is most pronounced for the higher injected flow rate which is represented by the upper curves. At the first location the concentration in the linear region of the flow is approximately $0.05C_i$ or 50 ppm. Mean concentration drops rapidly with distance from the wall to approximately $0.012C_i$ or 12 ppm at $y^+ = 100$. At the second location, the concentration is approximately 20 ppm near the wall and is approximately 9 ppm at $y^+ = 100$. the concentration profiles at the final two locations are nearly identical with the mean concentration at the third location varying from 6 ppm near the wall to 4 ppm at $y^+ = 100$ and at the fourth location from 5 ppm near the wall to 4 ppm at $y^+ = 100$.

The lower curves on Figure 6 represent the lower injected flow rate. At the first location the concentration varies from approximately 7.5 ppm near the wall to 5 ppm at $y^+ = 100$. At the second location $\bar{C}$ varies from approximately 4.5 ppm to 3 ppm across this same region. The mean concentration at the last two locations is very low. It varies from about 3 ppm to 2 ppm at the third location, and it is always less than 2 ppm at the final location. Profiles of the root mean square concentration for both cases are given in the appendix.

Poreh and Cermak (1964) studied the diffusion of a passive scalar injected from a slot into a two-dimensional Newtonian boundary layer. From their data they developed correlations for the injectant concentration at the wall for various regions of mixing. These correlations, when applied to the present data underpredict the measured concentration by as much as one order of magnitude. This result implies that drag reducing polymer inhibits the mixing process as has been observed by several previous authors. This result is consistent with measurements performed by Walker & Tiederman (1989b) for injection of the same polymer into a fully developed channel flow. The present results and those of Walker & Tiederman cannot be compared directly because they represent much different streamwise regions in the flow. A

number of authors have observed similar trends with other polymers. Fruman & Tulin (1976) and Vdovin & Smolyakov (1978) have studied and correlated the near-wall concentration for injection of polyethelene oxides into water. They both observed the same qualitative decrease in mixing. However, their correlations fail to predict the present data, probably because the polymers are different. Latto & El Reidy (1976) observed suppression for mixing by a polyacrylamide; however, their correlation for wall concentration does not predict the present data. It is unclear whether this difference is due to the fact that the polymer is not identical or whether it is due to a different method of injection.

In order to assess the influence of the near-wall polymer concentration on the local shear viscosity, the apparent steady shear viscosity for 10, 20 and 50 ppm homogeneous polymer solutions was measured using a Brookfield model LVT cone and plate viscometer. This instrument has a maximum strain rate of 230 s^{-1} which is approximately one third the mean wall strain rate in these flows. Because polyacrylamide solutions are shear thining, the effective shear viscosity at the wall for the present boundary layers is probably less than that measured with the viscometer. These tests showed that the effective steady shear viscosity of homogeneous polymer solutions is within 10 percent of the solvent viscosity at concentrations up to 20 ppm and a strain rate of 230 s^{-1}. At 50 ppm and the same strain rate, the viscosity indicated by the Brookfield is approximately 25 percent higher than that of the water. Therefore, the use of the solvent viscosity in the present shear stress measurements should introduce less than ten percent error for all experiments except $Q_i/Q_s = 2$ at the first location. For this case the error bound is less than 25 percent.

4.2 Velocity statistics

Figure 7 shows mean streamwise velocity profiles in inner normalized form at a single location for each polymer injection flow rate and for the corresponding Newtonian case. As before, the viscosity is assumed to be as that of the solvent. The Newtonian data clearly shows a logarithmic region which closely follows the standard log-law relationship with $\kappa = 0.41$ and $B = 5.0$. As the polymer injection flow rate increases, a log region still is evident, but the normalized velocities are distinctly higher than in the Newtonian case and the slope of the log region clearly increases with the injected flow rate. This same trend was observed at all measurement locations, as can be seen from the plots shown in the appendix. The upward shift in the data is a well established feature of polymer drag reduction (see e.g. Virk, 1975). The change in slope has been observed in well mixed, fully developed channel flows by Harder (1989), in heterogeneous pipe flows by Bewersdorff (1984) and in homogeneous flat plate boundary layers by Kumor & Sylvestor (1973).

Because few other studies have observed this change in slope, experiments were performed to prove that the observed change was not the result of polymer buildup in the recirculating channel water. In previous investigations using this flow loop (see Harder, 1989 and Walker & Tiederman, 1989b) the additives were degraded sufficiently by the centrifugal pumps that there was no evidence that the background accumulation of degraded polymer affected the results. In these experiments the amount of additive injected into the loop was considerable higher and additional precautions were taken. All velocity profiles in the present study were measured by traversing the LDV probe volume in steps outward from the wall. The velocity at a point in the logarithmic region of the corresponding Newtonian flow was monitored periodically throughout the experiment to determine if sufficient degraded polymer had accumulated in the channel to influence the boundary layer without injection. When the velocity

measured in the channel with no polymer injection changed from the original Newtonian case before any polymer entered the channel by more than 1.5 percent, the channel was drained and refilled with new water from a storage tank. This procedure ensured that the background concentration of polymer was effectively low, but does not by itself ensure that the observed change in slope is not due to some extreme sensitivity to polymer buildup. In order to eliminate this possibility, two of the high flow rate experiments were performed with the probe volume moving outward from the wall until it reached the outer reaches of the log region, $y^+ \cong 300$. The water in the channel was then changed to eliminate all residual polymer from the system and then three of the log region points were immediately repeated with the probe volume moved toward the wall. The measured velocity for these points was within one percent of that measured before the water change. These three points are plotted on Figure 7 along with the remainder of the data for the high flow rate. Note that these three points are hardly discernable from the rest of the data. The observed change in slope therefore does not result from polymer build up in the channel.

Figures 8 through 10 show the variation of the mean velocity, rms fluctuation, and Reynolds stress profiles with streamwise location during drag reduction. These profiles are for the lower injection flow rate. The higher flow rate exhibits the same trends. On each plot Newtonian data at $Re_\theta = 3527$, the third location, are shown for reference. The change of slope and offset of the logarithmic region of the mean velocity profile exist for all the streamwise locations, but the magnitude of each decreases with streamwise distance. This trend is at least qualitatively related to the decrease in mean concentration in the buffer region with streamwise distance.

Figure 9 shows the root mean square velocity profiles for the same set of data. In all the

drag-reduced cases, the peak in u'/u_τ increases in magnitude and moves outward from the wall compared to the Newtonian case. This difference is largest at the first location and the data move toward the Newtonian curve as the flow moves downstream. This change is clearly related to the drag reduction phenomenon; because, it is much greater than the small Reynolds number variation seen in the Newtonian boundary layer as is shown in the appendix. A number of investigators have previously observed an increase in both the magnitude and location of the normalized streamwise statistic in zero pressure gradient boundary layers (Fontaine et al.,1990), two-dimensional channels (Reichman & Tiederman, 1975; Willmarth et al, 1987; Luchik & Tiederman, 1988; Walker & Tiederman 1990; Harder, 1989), in two-dimensional open channel flows (Schmid, 1984) and in slot injection in developing boundary layers in ducts (Maksimovic, 1984). El Reidy & Latto (1984) found that slot injection of polymer solution into a zero pressure gradient boundary layer resulted in an increase in u' for injected concentrations of 500 ppm and 1000 ppm. In circular pipe flows, u' has been observed to increase (McComb & Rabie, 1982); although some authors found a decrease, (Mizushina & Usui, 1977; Bewersdorff, 1984).

The normal velocity fluctuation data, v'/u_τ is apparently unaffected by the polymer outside of $y^+ \cong 100$. Inside of $y^+ \cong 100$ the value of v'/u_τ is always somewhat reduced from the Newtonian value, but the magnitude of this change does not vary consistently with location. The Newtonian data also exhibits some apparently random variation with streamwise location. Therefore, it is certain that v'/u_τ, decreases in a drag-reduced boundary layer for $y^+ \leq 100$, but the magnitude of this variation with streamwise distance, which is relatively small, is not clearly defined by these experiments. The v' decrease has been observed in polymer drag-reduced flows in zero pressure gradient boundary layers (Fontaine et al.,1990), two-dimensional channels (Willmarth et al., 1987; Luchik & Tiederman, 1988; Walker and Tiederman, 1990; Harder,

1989), in developing duct flow (Maksimovic, 1984), and in pipe flow (Bewersdorff, 1984).

Figure 10 shows the variation of the Reynolds shear stress for the same data sets. There is a reduction in the the Reynolds stress for $y^+ \leq 50$ for all drag-reduced cases. The magnitude of this change is greatest at the first measurement location. There is no consistent change in the Reynolds stress between $y^+ \cong 50$ and $y^+ \cong 200$. Outside of this region the data do not collapse; however, these differences are basically due to Reynolds number influences which also occur in fully Newtonian cases. In particular note that there is little difference between the drag-reduced and Newtonian boundary layers at the same location, corresponding to $Re_\theta = 3527$. Other investigators have observed that the Reynolds shear stress decreases during drag reduction (Bewersdorff, 1984; Schmid, 1984; Willmarth et al., 1987; Luchik & Tiederman, 1988; Harder, 1989; Walker & Tiederman , 1990; Fontaine et al. 1990).

Figures 11 through 14 show profiles of the viscous and Reynolds shear stresses along with their sum at each streamwise location. The stresses are normalized by $\frac{1}{2}\rho U_e^2$, where ρ is the density and U_e is the freestream velocity. The location of each point normal to the wall is normalized using inner variables. The upper set of curves on each plot is for the high injection flow rate, the middle set of curves represents the low flow rate, and the bottom data are for an unmodified Newtonian boundary layer. The velocity data for each profiles were smoothed by a running five point, second order least squares fit in order to evaluate $d\overline{U}/dy$. The viscosity of water was always used in evaluating the viscous shear. In each Newtonian case, the normalized wall shear stress as determined from the log region of the flow, is indicated as a dot on the left axis of the plot. Figure 11 shows the stress distributions at the first measurement location. The Newtonian profile shows the expected distribution of stresses. The stress in the linear sublayer is essentially all viscous. The viscous stress component quickly diminishes and is negligible for

$y^+ \geq 50$. The magnitude of the Reynolds stress increases dramatically between $y^+ \cong 5$ and $y^+ \cong 50$ then is nearly constant until approximately $y^+ = 250$. Outside of this region the Reynolds stresses drop to zero. Most importantly, the sum of these two stress components, indicated by squares, is nearly constant from the wall to approximately $y^+ = 250$. Both polymer cases clearly have a different stress distribution than the Newtonian case. These flows, exhibits a region, $6 \leq y^+ \leq 100$, in which the sum of the viscous and Reynolds stresses is clearly less than the value either near the wall ($y^+ \leq 5$) or in the log region ($100 \leq y^+ \leq 250$). In addition, the sum of these stresses in the linear and log region are the same, within the accuracy of the measurements. However, because the freestream pressure gradient remains zero in the drag reduced case, the total stress should remain constant from the wall through the log region. There is no mechanism by which the total normalized stress would be lower in magnitude in the buffer region than in the linear and log regions. The behavior of the stresses at the second measurement location exhibits similar trends although the apparent total stress deficit between $6 \leq y^+ \leq 100$ is not as large. There appears to be a small stress deficit at the third location; however, the existence of the deficit is not as distinct. At the farthest downstream measurement station, shown in Figure 14, there is no longer a detectable stress deficit for either drag reduction case. Harder detected a similar apparent total stress deficit in a homogeneous fully developed polymer drag-reducing, two-dimensional channel flow of the same polymer when the polymer concentration and wall stain rate were 5 ppm and 4000 s^{-1}. Willmarth et al. and Bewersdorf have also found that the sum of the Reynolds stress and viscous shear stresses do not always add up to the expected distribution.

In order to prove that this apparent stress deficit is directly related to the presence of the polymer in the boundary layer, an experiment was performed in which two component velocity

profiles were measured at $x/\delta_s = 52$ with no injection, with water injection at $Q_i/Q_s = 1$, and with water injection at $Q_i/Q_s = 2$. There was no measurable change in the mean velocity and the rms velocity fluctuations when water was injected at either flow rate. There was also no apparent change in the magnitude of the Reynolds stress with water injection. However, the scatter in the Reynolds stress increased slightly as the injection flow rate increased. These profiles are shown in the appendix. These experiments clearly prove that the apparent stress deficit observed in the drag reduction experiments is a result of the existence of polymer in the boundary layer and is not a result of the injection process itself.

The apparent stress deficit probably occurs only in the region $5 \leq y^+ \leq 100$ because of the extensional nature of the flow in this region. Gyr (1984) proposed that drag reduction occurs when the polymer molecules are stretched by an extensional flow. In the linear sublayer , $y^+ \leq 5$, the polymer is probably not activated because the flow is essentially viscous and not extensional. Outside of the buffer region $y^+ \geq 100$, the extensional motions in the flow are weaker and at the same time the polymer concentration decreases. Therefore, the polymer molecules are less likely to be activated. This hypothesis is consistent with results of Tiederman et al. (1985) who found that the polymer is basically passive inside $y^+ = 10$ It is also consistent with the observation of McComb & Rabie (1982) that the polymer is apparently passive if it is outside $y^+ = 100$.

5. Conclusions

There are two major conclusions from the present data. First, the sum of the viscous shear and Reynolds stresses in polymer drag-reduced boundary layers does not always account for the total shear stress in the boundary layer. Some other stress which is a result of the polymer may

be apparently present. The second is that the slope of the logarithmic region of a polymer drag-reduced flow may increase over the Newtonian slope. The latter feature may depend on the type of polymer additive.

6. References

BEWERSDORFF, H.W. 1984 Heterogene widerstandsverminderung bei turbulenten rohrstromungen. *Rheologica Acta, 23,* 522-543.

COLES, D.E. 1962 *The turbulent boundary layer in a compressible fluid.* Rand report R-403-PR.

COLES, D.E. 1968 The Young Peoples Guide to the Data. In: *Proceedings Computation of Turbulent Boundary Layers, vol. II,* D.E. Coles and E.A. Hirst, eds., Stanford Univ., 1-19.

ERM, L.P.;SMITS, A.J. & JOUBERT, P.N. 1985 Low Reynolds number turbulent boundary layers on a smooth flat surface in a zero pressure gradient. *5th Int. Symp. Turb. Shear* Cornell

EL REIDY, O.K. & LATTO, B. 1984 Energy spectra and turbulence intensity polymer injection flows. In: *Drag Reduction,* R.J.H Sellin and R.T.Moses, eds., Univ. of Bristol, B.5.

FONTAINE, A.A.; PETRIE, H.L. & BRUNGART, T.A. 1990 Turbulent boundary layer velocity profile statistics with slot injected drag reducing polymers. Penn State Univ. report 90-279.

FRUMAN, D.H. & TULIN M.P. 1976 Diffusion of a tangential drag-reducing polymer injection on a flat plate at high Reynolds numbers. *J. Ship Research, 20,* 171-180.

GYR, A. 1984 Direct evidence that drag reduction in an effect of the elongation of polymer molecules. *Drag reduction in fluid flows,* R.J.H. Sellin and R.T. Moses eds., Univ. Bristol, paper B10.

HARDER, K.J. 1989 Influence of wall strain rate, polymer concentration and channel height upon drag reduction and turbulent structure. MS thesis, Purdue University.

KUMOR, S.M. & SYLVESTER N.D. 1973 Effects of a drag-reducing polymer on the turbulent boundary layer. *AIChE Symposium Series, 130,* vol. 69,1-13

LATTO, B. & EL REIDY O.K. 1976 Diffusion of polymer additives in a developing turbulent boundary layer. *J. Hydronautics,* 10, 135-139.

LUCHIK T.S. & TIEDERMAN W.G. 1987 Timescale and structure of ejections and bursts in turbulent channel flows. *J. Fluid Mech.,174,* 529-552.

LUCHIK T.S. & TIEDERMAN W.G. 1988 Turbulent structure in low-concentration drag-reducing channel flows. *J. Fluid Mech.,* 190, 241-263.

MAKSIMOVIC, C. 1984 Turbulence structure of a developing duct flow with near-wall injection of drag reduction. In: *The Influence of Polymer Additives on Velocity and Temperature Fields.* B. Gampert ed., Springer-Verlag, 359-368.

McCOMB, W.D. & RABIE, L.H. 1982 Local drag reduction due to injection of polymer solutions into turbulent flow in a pipe, part I: dependence on local polymer concentration; part II: laser-Doppler measurements of turbulent structure. *AIChE J., 28*, 547-565.

MIZUSHINA, T. & USUI, H. 1977 Reduction of eddy diffusion for momentum and heat in viscoelastic fluid flow in a circular pipe. *Phys. Fluids, 20*, S100-S108.

MURLISS, J.; TSAI, H.M., & BRADSHAW, P. 1982 The structure of turbulent boundary layers at low Reynolds numbers. *J. Fluid Mech., 122*, 13-56.

POREH, M. & CERMAK, J.E. 1964 Study of diffusion from a line source in a turbulent boundary layer. *Int. J. Heat Mass Trans., 7*, 1083-1095.

PURTELL, L.P., KLEBANOFF, P.S. & BUCKLEY, F.T. 1981 Turbulent boundary layer at low Reynolds number. *Phys. Fluids, 24*, 802-811.

REISCHMAN M.M. & TIEDERMAN, W.G. 1975 Laser-Doppler anemometer measurements in drag-reducing channel flows. *J. Fluid Mech., 70*, 369-392.

SCHMID A. 1984 Experimental investigation of drag reducing polymers on a turbulent channel flow. *Drag Reduction*, R.J.H Sellin and R.T.Moses, eds., Univ. of Bristol, B.12.

SHAH, D.A. & ANTONIA, R.A. 1989 Scaling of the "bursting" period in turbulent boundary layer and duct flows. *Phys. Fluids A, 1*, 318-325.

TIEDERMAN, W.G.; LUCHIK, T.S. & BOGARD D.G. 1985 Wall-layer structure and drag reduction. *J. Fluid Mech., 156*, 419-437.

VIRK, P.S. 1975 Drag reduction fundamentals. *AIChE J., 21*, 625-656.

VDOVIN, A.V. & SMOL'YAKOV, A.V. 1978 Diffusion of polymer solutions in a turbulent boundary layer. *J. Appl. Mech. Tech. Phys. 19*, 66-73, Engl. trans. 196-201.

WALKER, D.T. & TIEDERMAN, W.G. 1989a Simultaneous laser velocimeter and concentration measurement. *J. Laser Applications, 1*, 44-48.

WALKER, D.T. & TIEDERMAN, W.G. 1989b The concentration field in a turbulent channel flow with polymer injection at the wall. *Exp. Fluids, 8*, 86-94.

WALKER, D.T. & TIEDERMAN, W.G. 1990 Turbulent structure in a channel flow with polymer injection at the wall. *J. Fluid Mech., 218*, 377-403.

WILLMARTH, W.W., WEI, T. & LEE, C.O. 1987 Laser anemometer measurements of Reynolds stress in a turbulent channel flow with drag reducing polymer additives. *Phys. Fluids, 30*, 933-935.
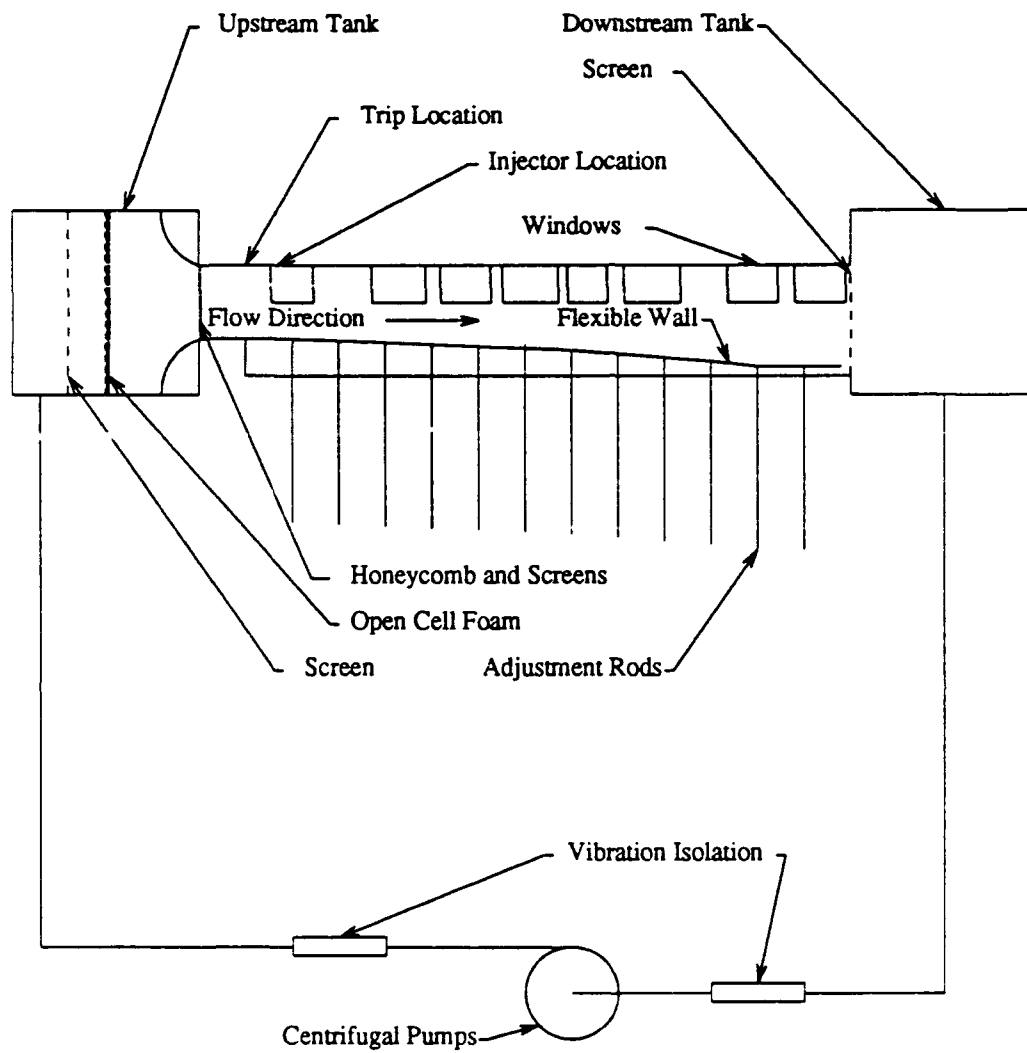
Figure 1.   Schematic diagram of the boundary layer facility.
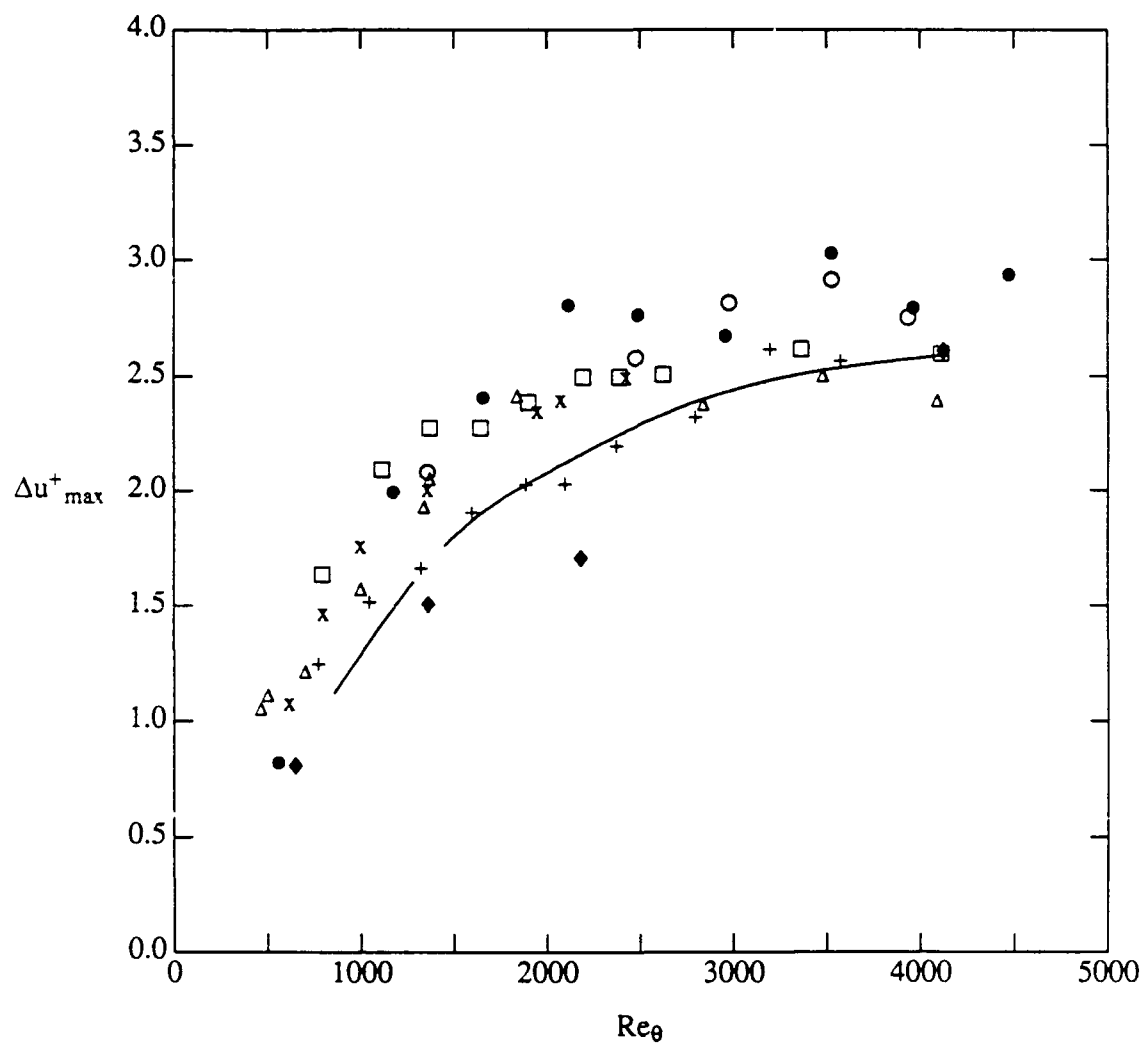
Figure 2.   Plot of the wake parameter,Δu^+ as a function of Re_θ for Newtonian boundary layers. o present study; ∆ Purtell et. al. (1981); □ Murliss et al. (1982); x Erm et al. (1985) (8 m/s); + Erm et al. (14 m/s); ◆ Shah & Antonia (1989); ● Wieghardt (Coles re-analysis, 1967); — Coles (1962).
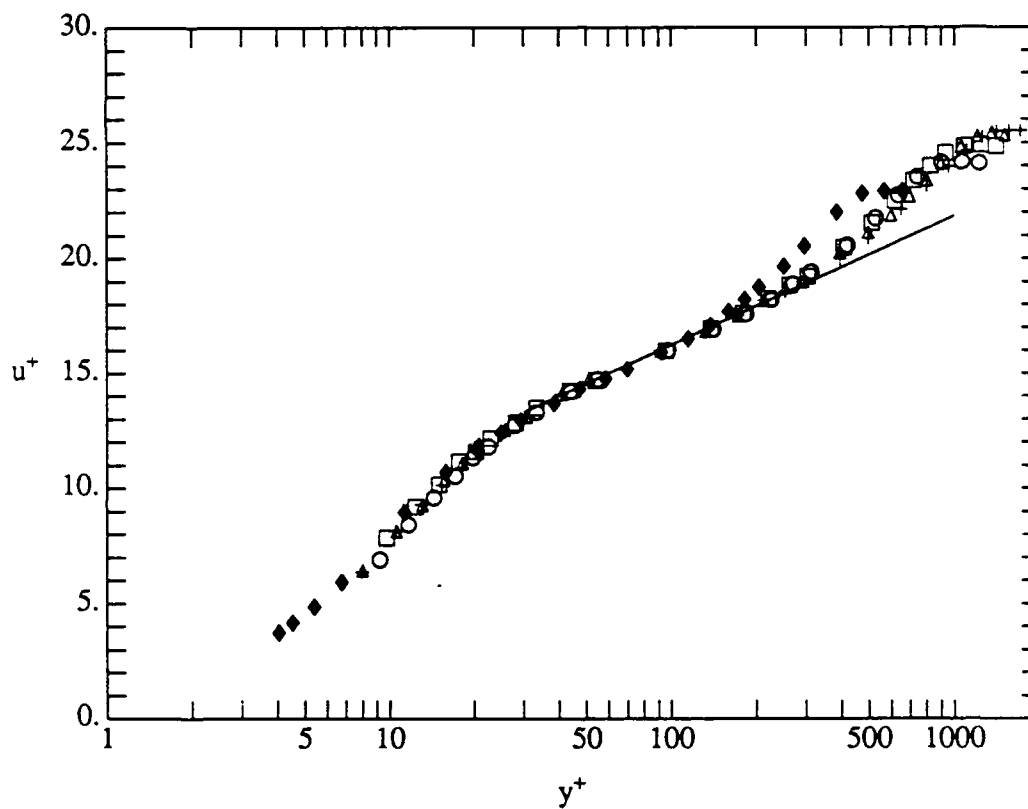
Figure 3.   Mean streamwise velocity in a Newtonian zero pressure gradient boundary layer without injection. ♦ Re_θ =1358; o Re_θ = 2478; □ Re_θ = 2978; Δ Re_θ = 3527; + Re_θ = 3935.
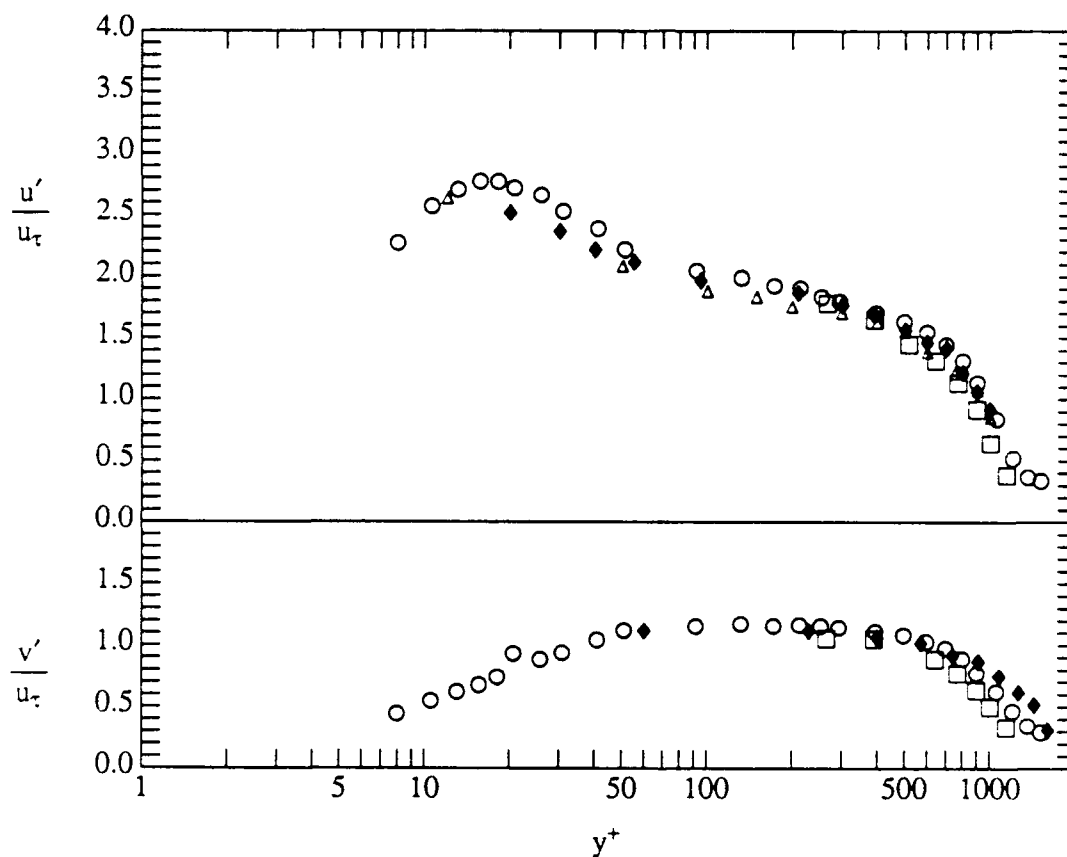
Figure 4.   Comparison of root-mean-square velocity statistics in Newtonian zero pressure gradient boundary layers without injection. O present Newtonian data $Re_\theta = 3527$; ▵ Purtell et al. $Re_\theta = 3480$; ♦ Erm et al. $Re_\theta = 3575$; ☐ Murliss et al. $Re_\theta = 3362$.
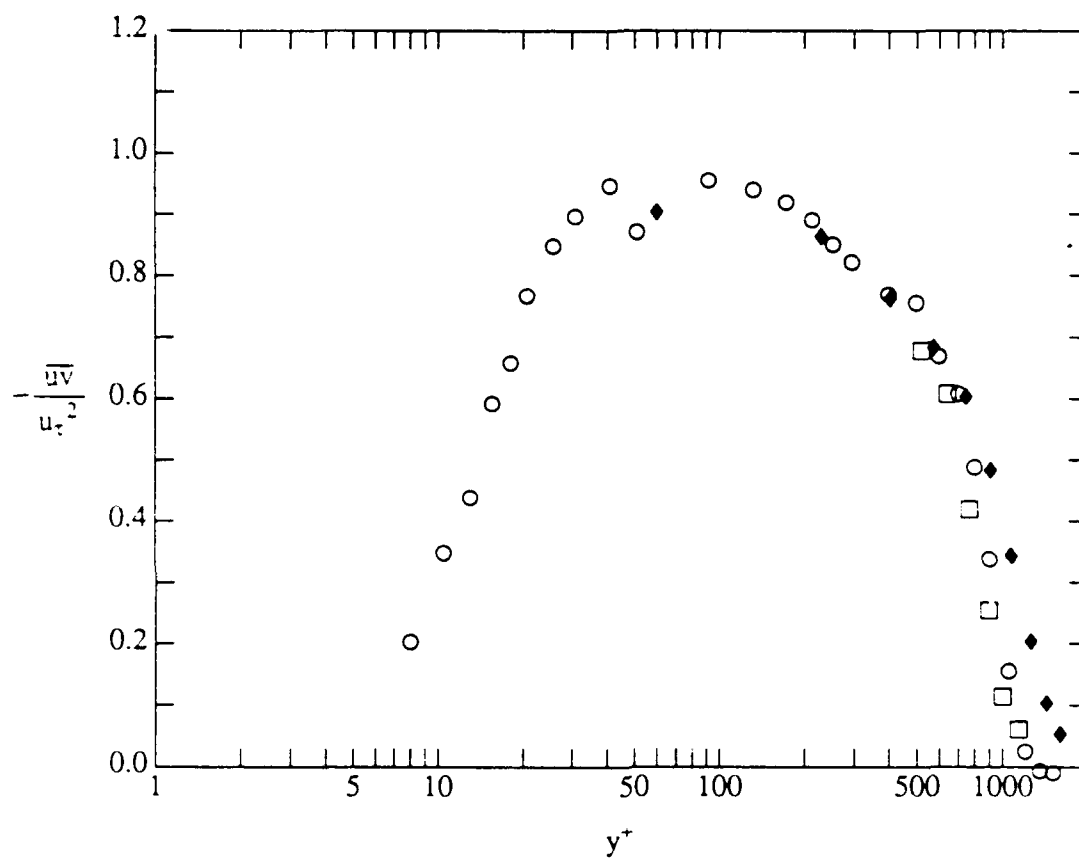
Figure 5.   Comparison of Reynolds shear stress in Newtonian zero pressure gradient boundary layers without injection. O present Newtonian data $Re_\theta = 3527$; ◆ Erm et al. $Re_\theta = 3575$; ❑ Murliss et al. $Re_\theta = 3362$.
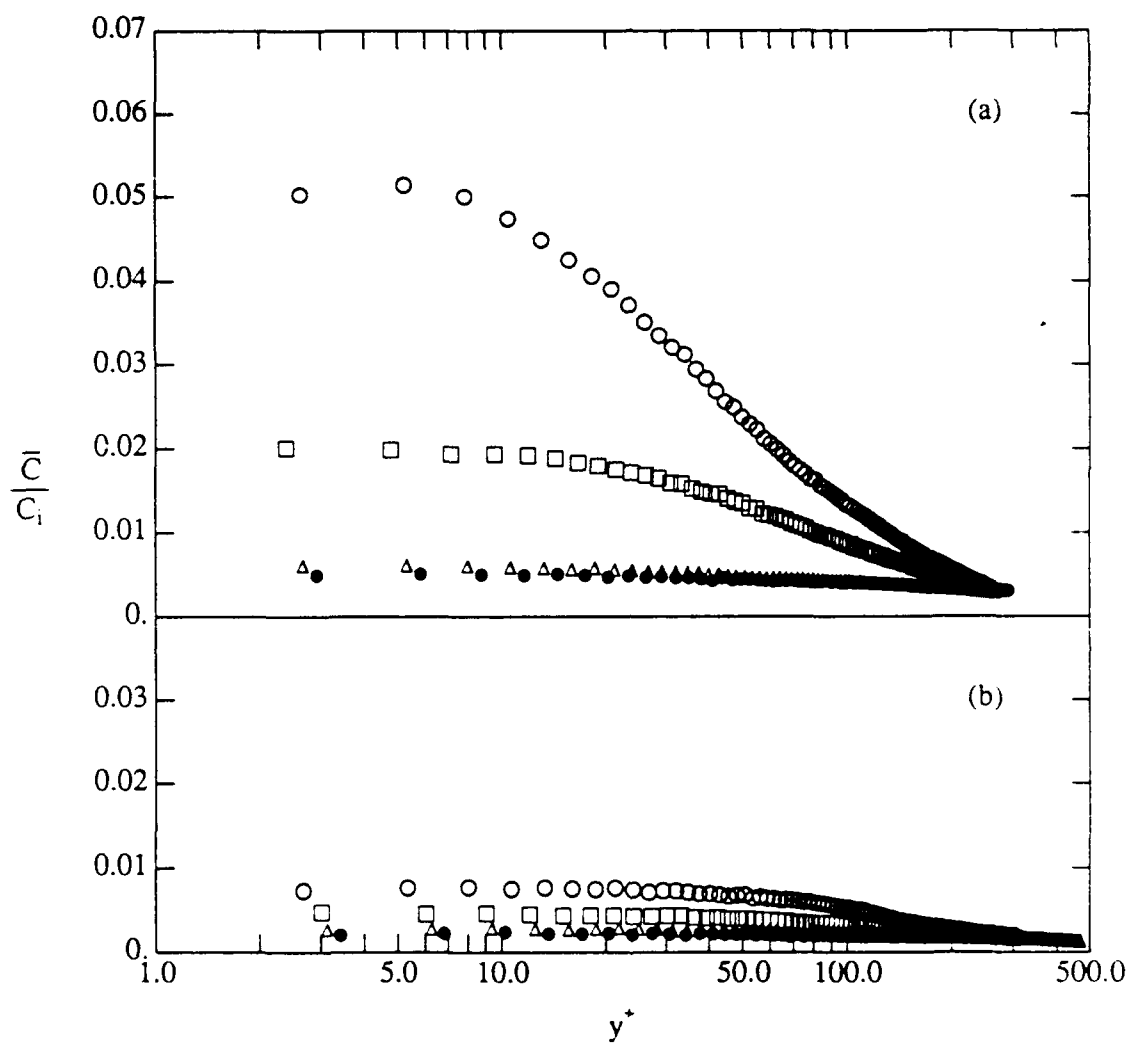
Figure 6.   Average polymer concentration normalized by the injected concentration. (a):
$Q_i/Q_s = 2$ (b): $Q_i/Q_s = 1$. ○ $Re_\theta|_N = 2478$, $x/\delta_s = 52$, $x^* = 29000$;
□ $Re_\theta|_N = 2978$, $x/\delta_s = 77$, $x^* = 43200$;
△ $Re_\theta|_N = 3527$, $x/\delta_s = 115$, $x^* = 64400$;
● $Re_\theta|_N = 3935$, $x/\delta_s = 144$, $x^* = 81000$;
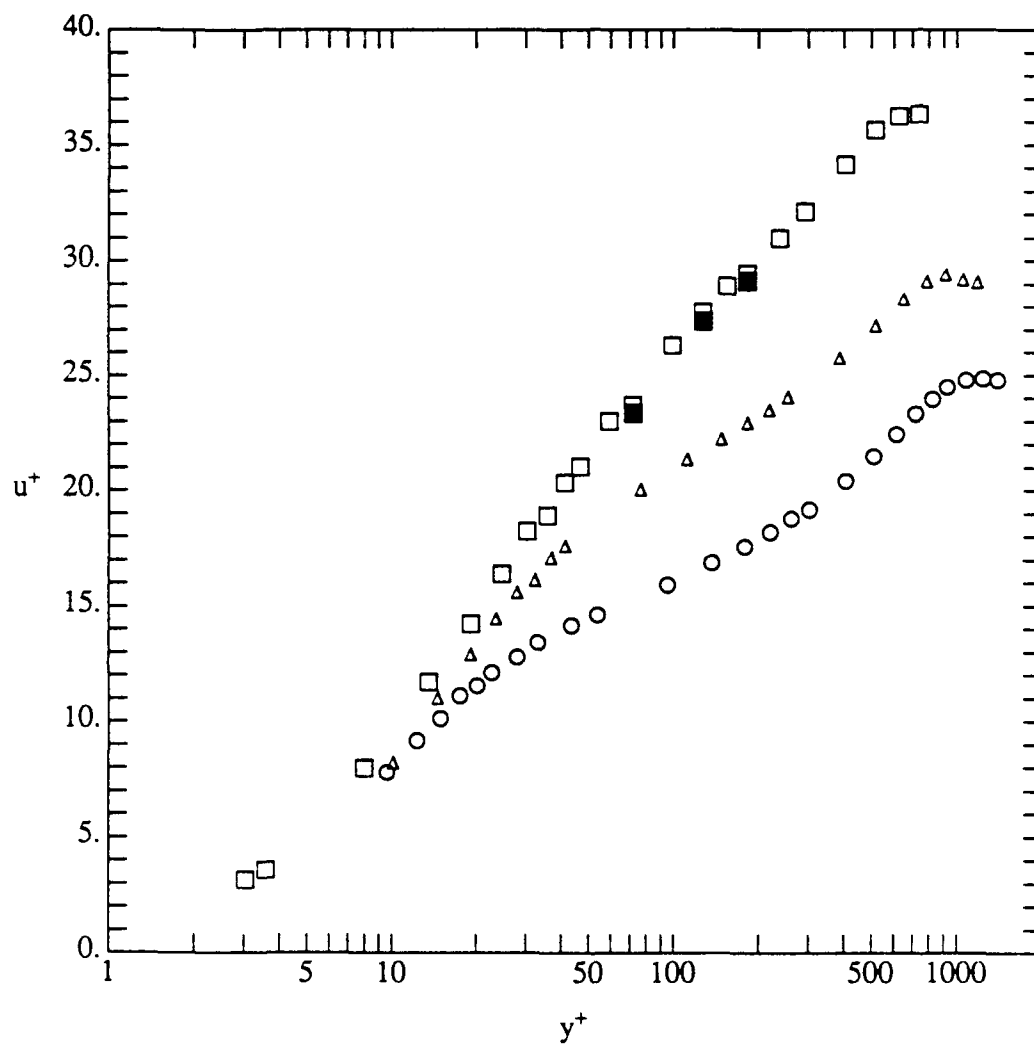
Figure 7.   Mean streamwise velocity in zero pressure gradient boundary layers comparing
             drag reduced flows to the Newtonian case at $Re_\theta |_N = 2978$, $x/\delta_s = 77$, $x^* = 43200$
             o $Q_i/Q_s = 0$; △ $Q_i/Q_s = 1$; □ $Q_i/Q_s = 2$; ■ $Q_i/Q_s = 2$ repeated point.
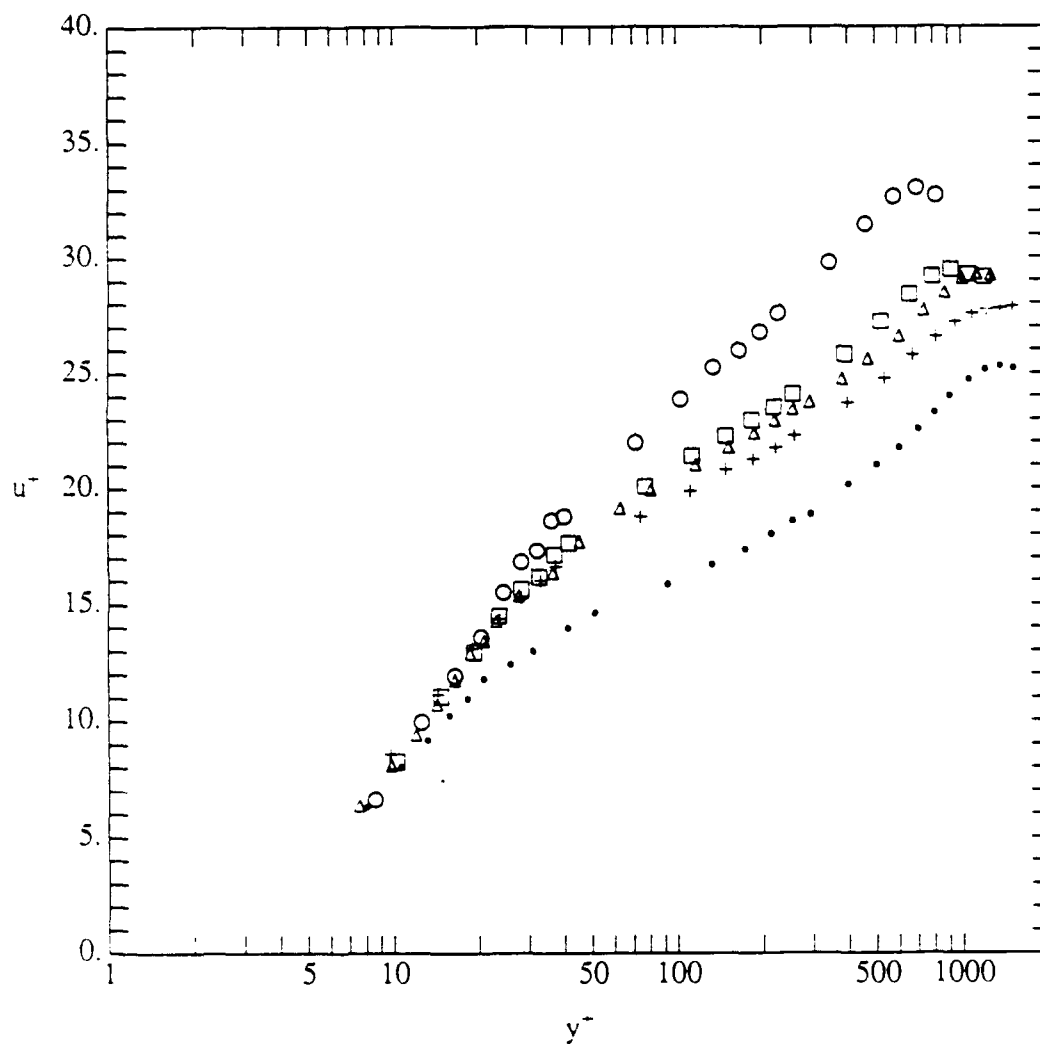
Figure 8.   Mean streamwise velocity for a drag reduced zero pressure gradient boundary layer with $Q_j/Q_s = 1$. o $Re_\theta|_N = 2478$, $x/\delta_s = 52$, $x^+ = 29000$;

□ $Re_\theta|_N = 2978$, $x/\delta_s = 77$, $x^+ = 43200$;

Δ $Re_\theta|_N = 3527$, $x/\delta_s = 115$, $x^+ = 64400$;

+ $Re_\theta|_N = 3935$, $x/\delta_s = 144$, $x^+ = 81000$; • $Re_\theta|_N = 3527$, $x/\delta_s = 115$, Newtonian, no injection.
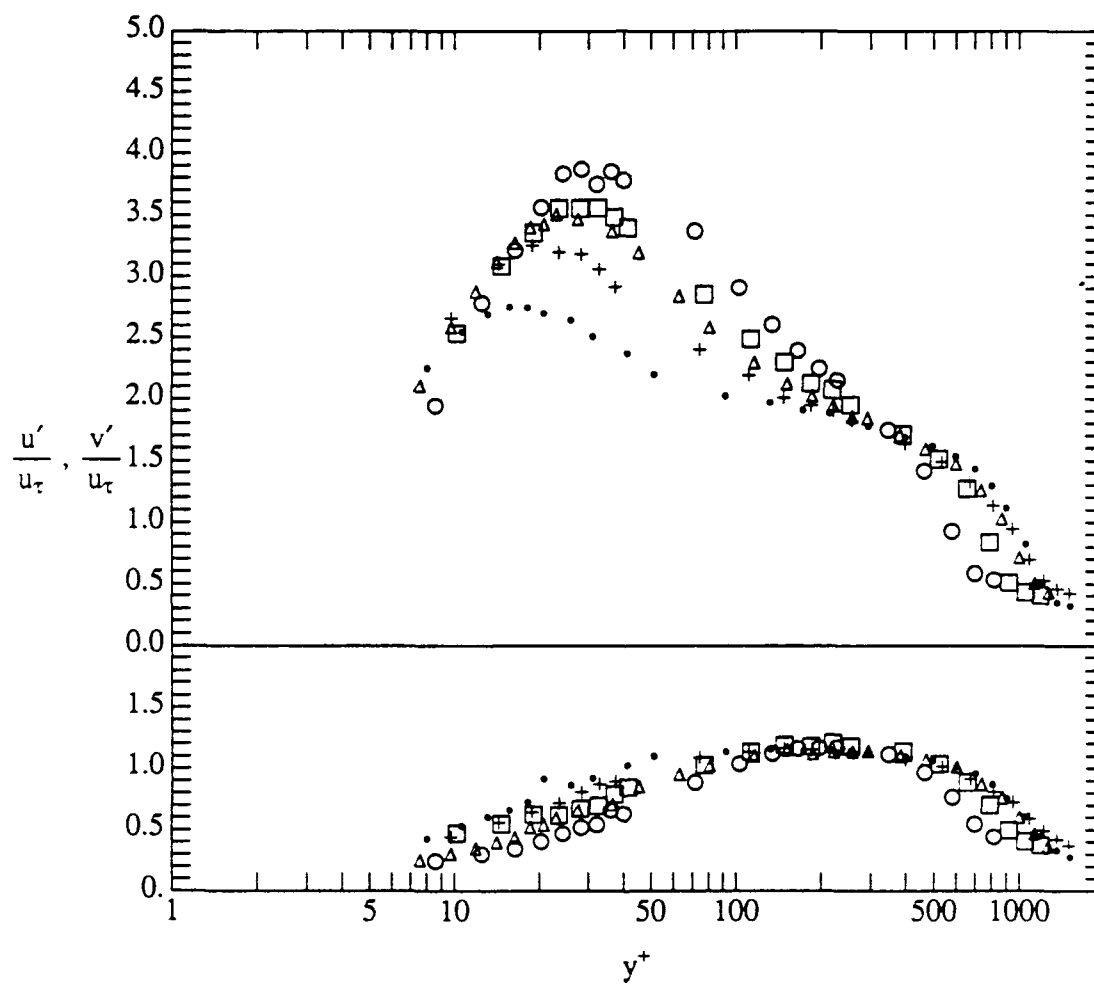
Figure 9.   Root-mean-square streamwise and normal velocity fluctuations for a drag reduced
zero pressure gradient boundary layer with $Q_i/Q_s = 1$.

o $Re_\theta|_N = 2478$, $x/\delta_s = 52$, $x^+ = 29000$;

□ $Re_\theta|_N = 2978$, $x/\delta_s = 77$, $x^+ = 43200$;

△ $Re_\theta|_N = 3527$, $x/\delta_s = 115$, $x^+ = 64400$;

+ $Re_\theta|_N = 3935$, $x/\delta_s = 144$, $x^+ = 81000$; • $Re_\theta|_N = 3527$, $x/\delta_s = 115$,
Newtonian, no injection.
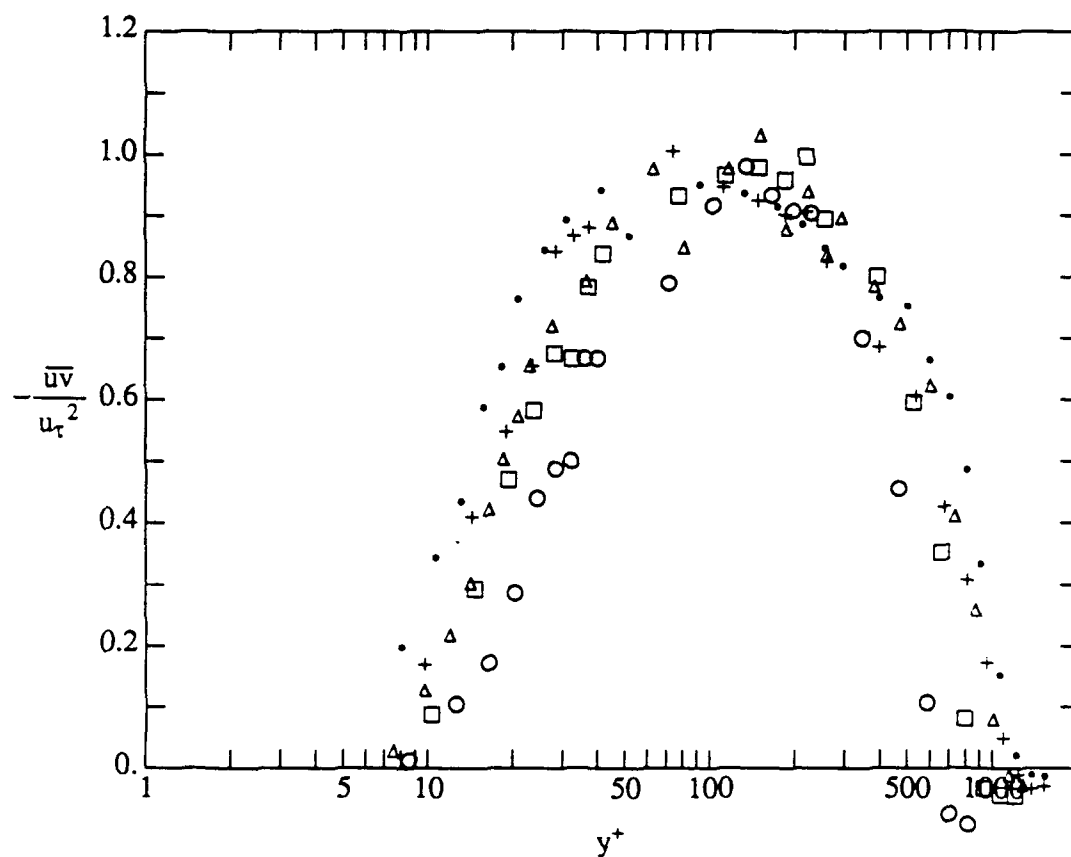
Figure 10.   Reynolds shear stress for a drag reduced zero pressure gradient boundary layer
with $Q_j/Q_s = 1$. ○ $Re_\theta |_N = 2478$, $x/\delta_s = 52$, $x^+ = 29000$;

□ $Re_\theta |_N = 2978$, $x/\delta_s = 77$, $x^+ = 43200$;

△ $Re_\theta |_N = 3527$, $x/\delta_s = 115$, $x^+ = 64400$;

+ $Re_\theta |_N = 3935$, $x/\delta_s = 144$, $x^+ = 81000$; • $Re_\theta |_N = 3527$, $x/\delta_s = 115$,
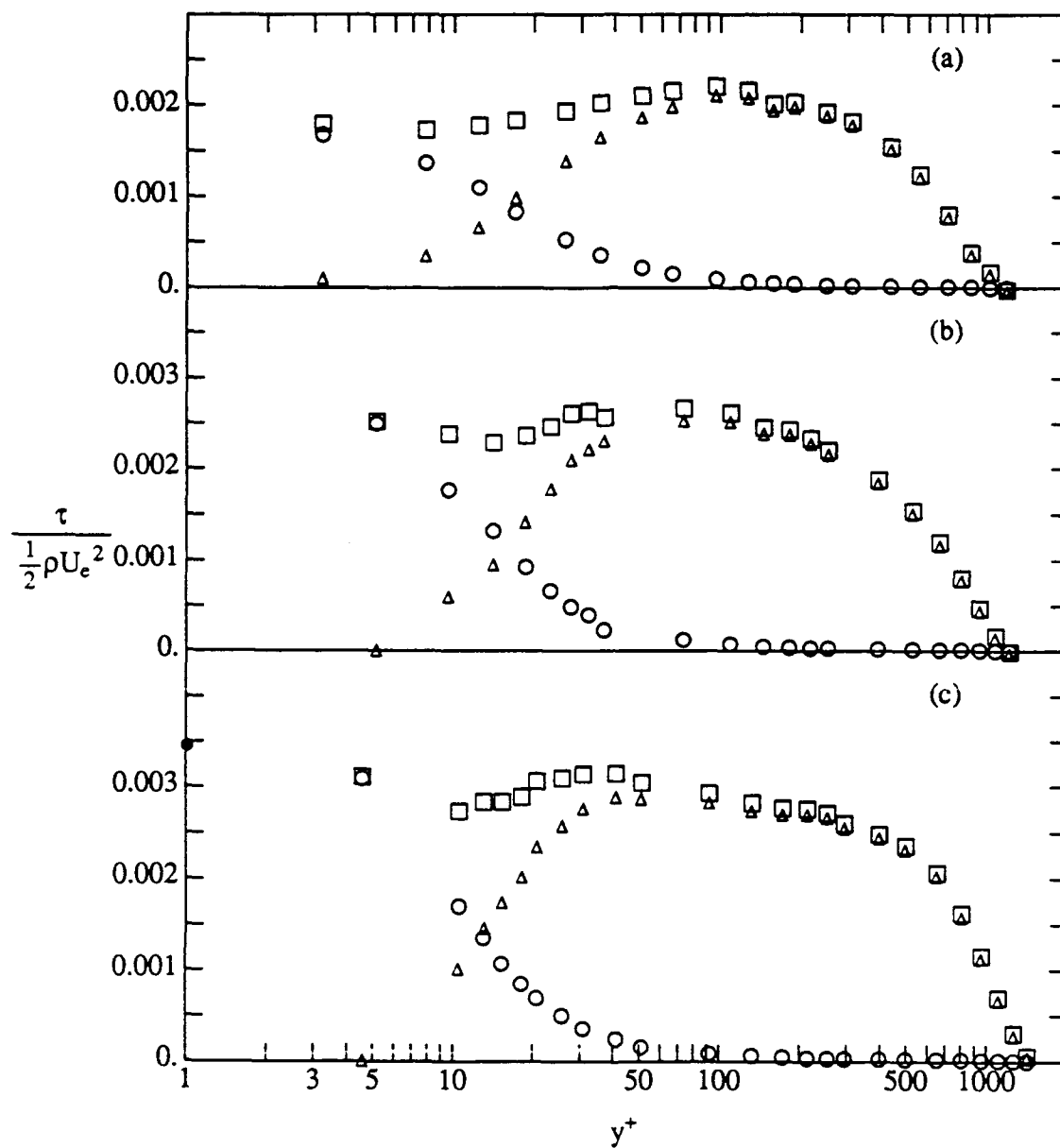Newtonian, no injection.
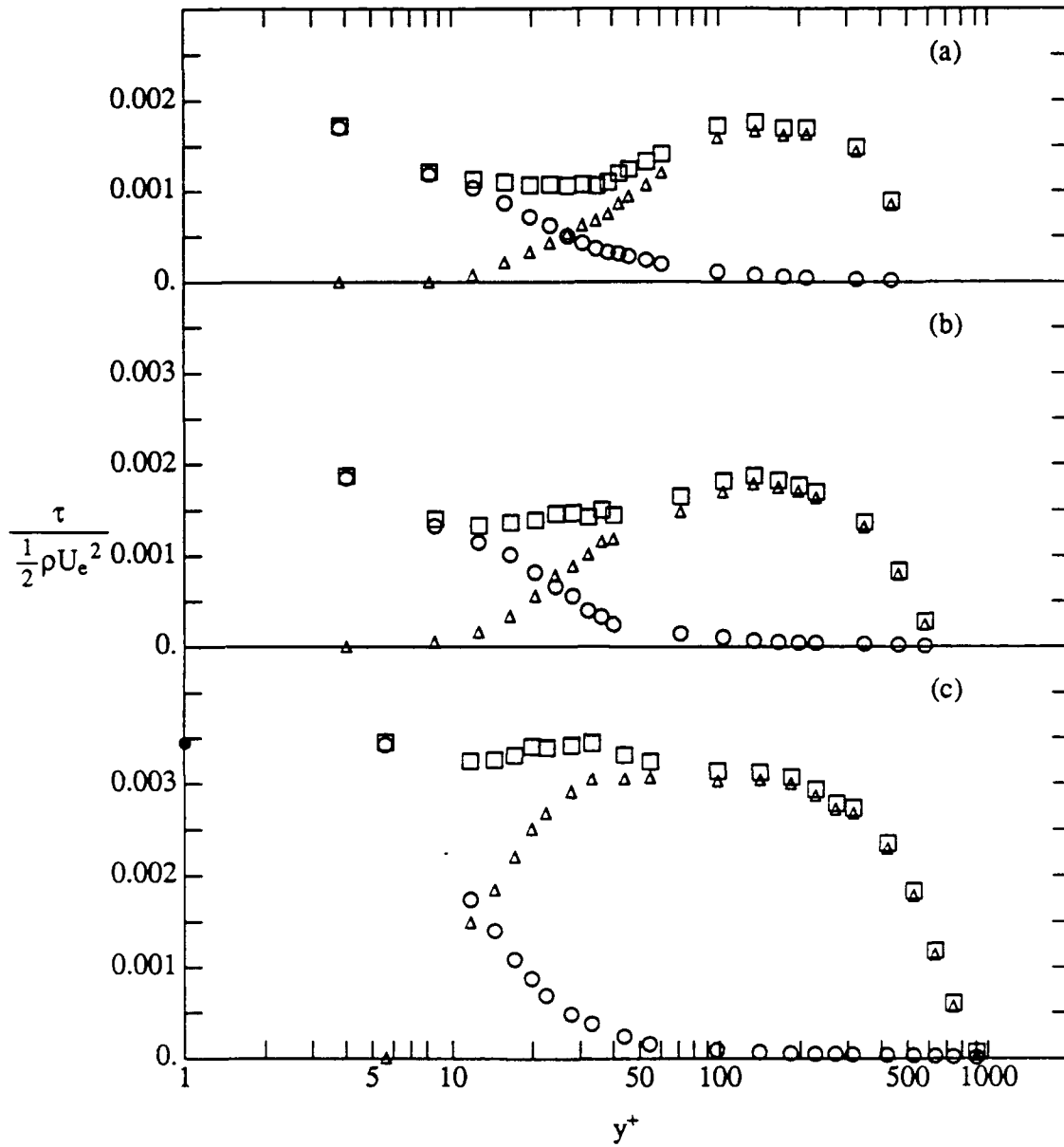
Figure 11. Shear stress in a zero pressure gradient boundary layer with and without polymer injection. $Re_\theta|_N = 2478$, $x/\delta_s = 52$, $x^* = 29000$. (a): $Q_i/Q_s = 2$; (b): $Q_i/Q_s = 1$; (c): no injection. o viscous shear stress $(\mu d\overline{U}/dy)$; $\triangle$ Reynolds stress $(-\rho\overline{uv})$; $\square$ sum of viscous and Reynolds stress; $\bullet$ Wall shear stress determined from the log region.
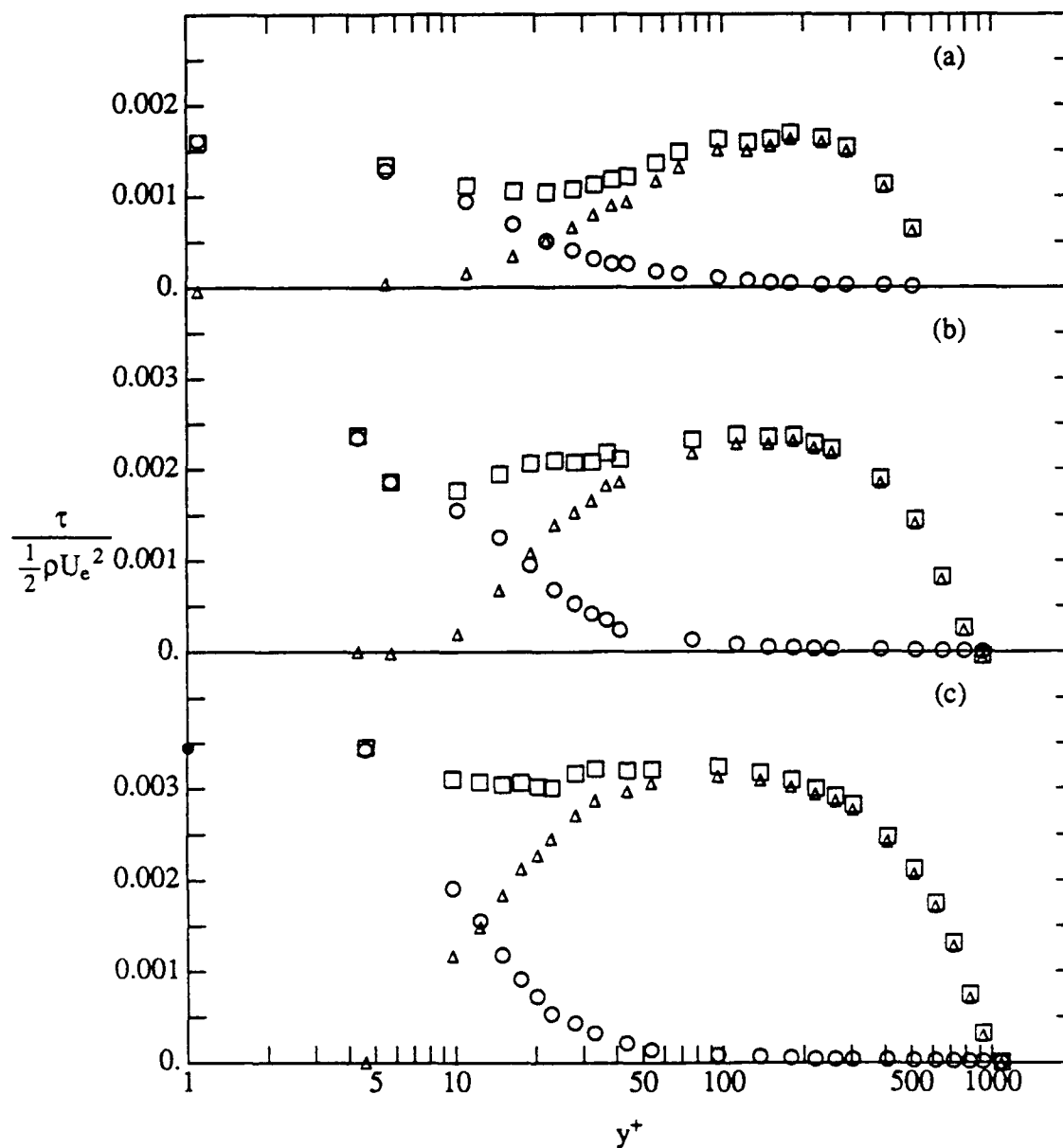
Figure 12.   Shear stress in a zero pressure gradient boundary layer with and without polymer injection. $Re_\theta |_N = 2978$, $x/\delta_s = 77$, $x^+ = 43200$. (a): $Q_i/Q_s = 2$; (b): $Q_i/Q_s = 1$; (c): no injection. o viscous shear stress ($\mu d\tilde{U}/dy$); $\triangle$ Reynolds stress ($-\rho\overline{uv}$); $\square$ sum of viscous and Reynolds stress; $\bullet$ Wall shear stress determined from the log region.
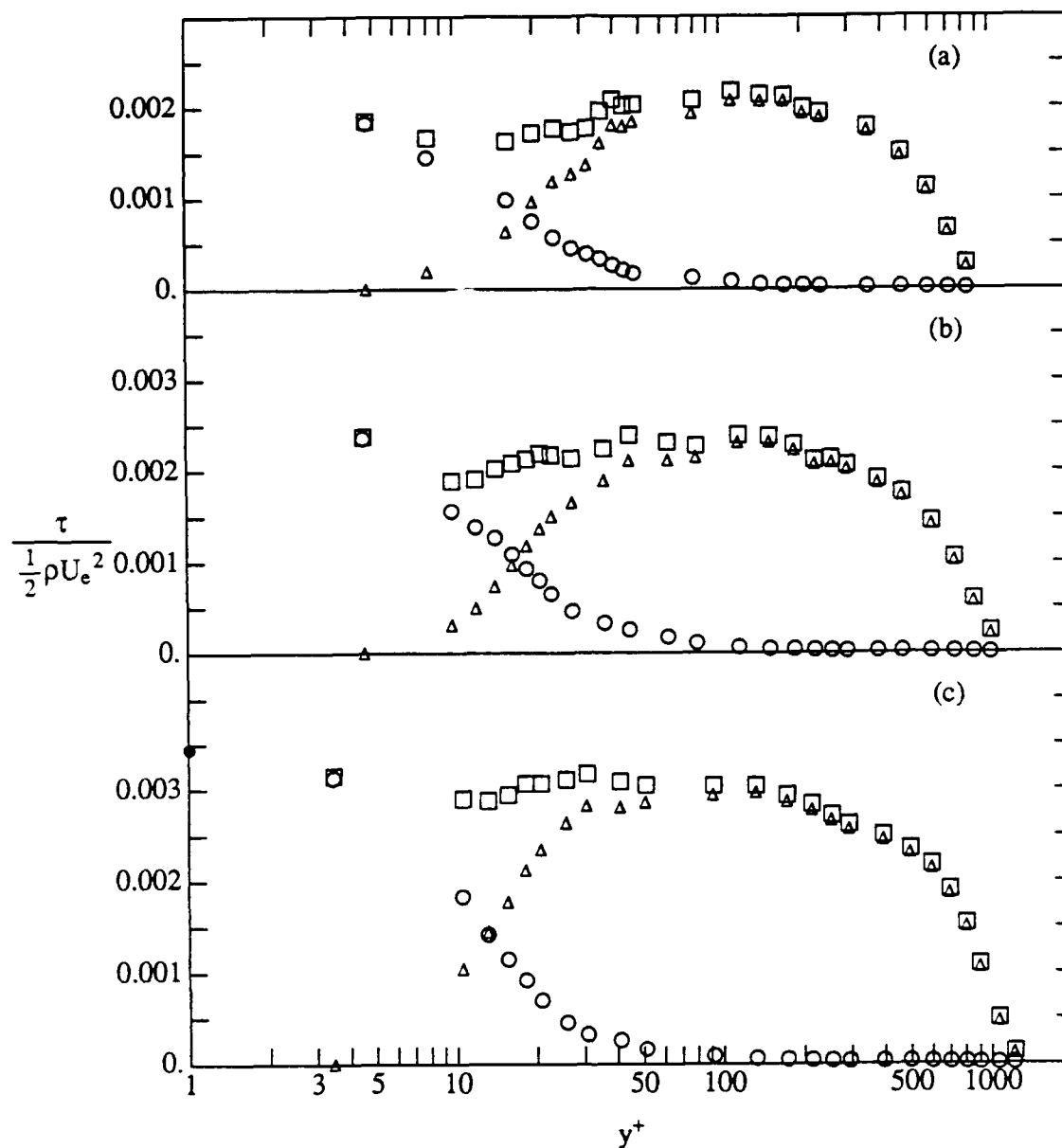
Figure 13. Shear stress in a zero pressure gradient boundary layer with and without polymer injection. $Re_\theta|_N = 3527$, $x/\delta_s = 115$, $x^* = 64400$. (a): $Q_i/Q_s = 2$; (b): $Q_i/Q_s = 1$; (c): no injection. o viscous shear stress ($\mu d\overline{U}/dy$); Δ Reynolds stress ($-\rho\overline{uv}$); □ sum of viscous and Reynolds stress; • Wall shear stress determined from the log region.

Figure 14.   Shear stress in a zero pressure gradient boundary layer with and without polymer injection. $\text{Re}_\theta\,|_N = 3935$, $x/\delta_s = 144$, $x^+ = 81000$. (a): $Q_i/Q_s = 2$; (b): $Q_i/Q_s = 1$; (c): no injection. o viscous shear stress ($\mu d\overline{U}/dy$); Δ Reynolds stress ($-\rho\overline{uv}$); □ sum of viscous and Reynolds stress; ● Wall shear stress determined from the log region.

7. Appendix

This appendix presents data which are not specifically shown in the main text. The first part of the appendix is a table summarizing the primary data of the study. Following the table are plots of the additional data.

The first section of figures summarizes the Newtonian data. Unless otherwise noted all these data were acquired with no injection of fluid into the boundary layer. Plots A.1 and A.2 compare the present data for shape factor, H, and skin friction coefficient, c_f, respectively, to Coles' (1962) correlations and to various recent data. All the data used for comparison have alreay been mentioned in the main test. The next two plots show the inner normalized velocity fluctuation statistics (A.3) and Reynolds stresses (A.4) for all the Newtonian data. The corresponding plot of mean velocity was shown in the main text as figure 3. The Reynolds stresses at the lowest Reynolds number $Re_\theta = 1358$ appear to be somewhat high in the log region of the flow. These data were replicated during a second experiment, so that they are not a measurement error. It is possible that they represent a slight influence of upstream conditions. The next three plots show inner normalized mean velocity (A.5a), rms fluctuation (A.5b), and Reynolds stress (A.5c) profiles for injection of water into the boundary layei. Each plot contains data for no injection, $Q_i/Q_s = 1$ and $Q_i/Q_s = 2$. These plots indicate that injection of plain water has no influence on these statistics except for a small increase in the scatter of the Reynolds stress. However, it does not appear that the true magnitude of the Reynolds stress, around which the data scatter, changes significantly.

The second set of plots is a complete set of inner normalized velocity statistical data for the polymer flows. Figures A.6 to A.9 present the full velocity statistics for each individual location. Each figure presents inner normalized mean velocity (part a), rms fluctuation (part b),

and Reynolds stress (part c) profiles for a single location. Each plot shows data for both polymer injection flowrates. Also included on each plot is the Newtonian data with no injection for the same location. The final figure (A.10) shows the root mean square concentration profiles for all locations and both injected flow rates.

Table 1 Summary of Newtonian data

$(x - x_{trip})$ (mm)	$(x - x_s)$ (mm)	U_e (m/s)	C_f	ΔU^+	δ^* (mm)	θ (mm)	Re_θ
181	47	0.9898	0.00393	2.36	1.95	1.32	1358
754	620	0.9815	0.00343	2.58	3.44	2.43	2478
1058	924	0.9746	0.00325	2.81	4.11	2.94	2978
1513	1379	0.9694	0.00313	2.91	4.90	3.50	3527
1867	1733	0.9790	0.00309	2.75	5.36	3.86	3935

Table 2 Summary of $Q_i/Q_s = 1$ data

$(x - x_s)$ (mm)	x/δ_s	x^+	U_e (m/s)	C_f	ΔU^+	δ^* (mm)	θ (mm)	Re_θ
620	52	29000	0.976	0.00185	0.69	3.25	2.20	2250
924	77	43200	0.980	0.00235	1.14	3.32	2.36	2412
1379	115	64400	0.978	0.00236	1.39	4.17	3.05	3107
1733	144	81000	0.970	0.00260	1.30	4.11	3.06	3091

Table 3 Summary of $Q_i/Q_s = 2$ data

$(x - x_s)$ (mm)	x/δ_s	x^+	U_e (m/s)	C_f	ΔU^+	δ^* (mm)	θ (mm)	Re_θ
620	52	29000	0.977	0.0017	0.61	3.17	2.06	2091
924	77	43200	0.961	0.0017	0.70	3.41	2.31	2320
1379	115	64400	0.992	0.0021	0.91	3.86	2.74	2830
1733	144	81000	0.945	0.0015	0.62	5.16	3.68	3620
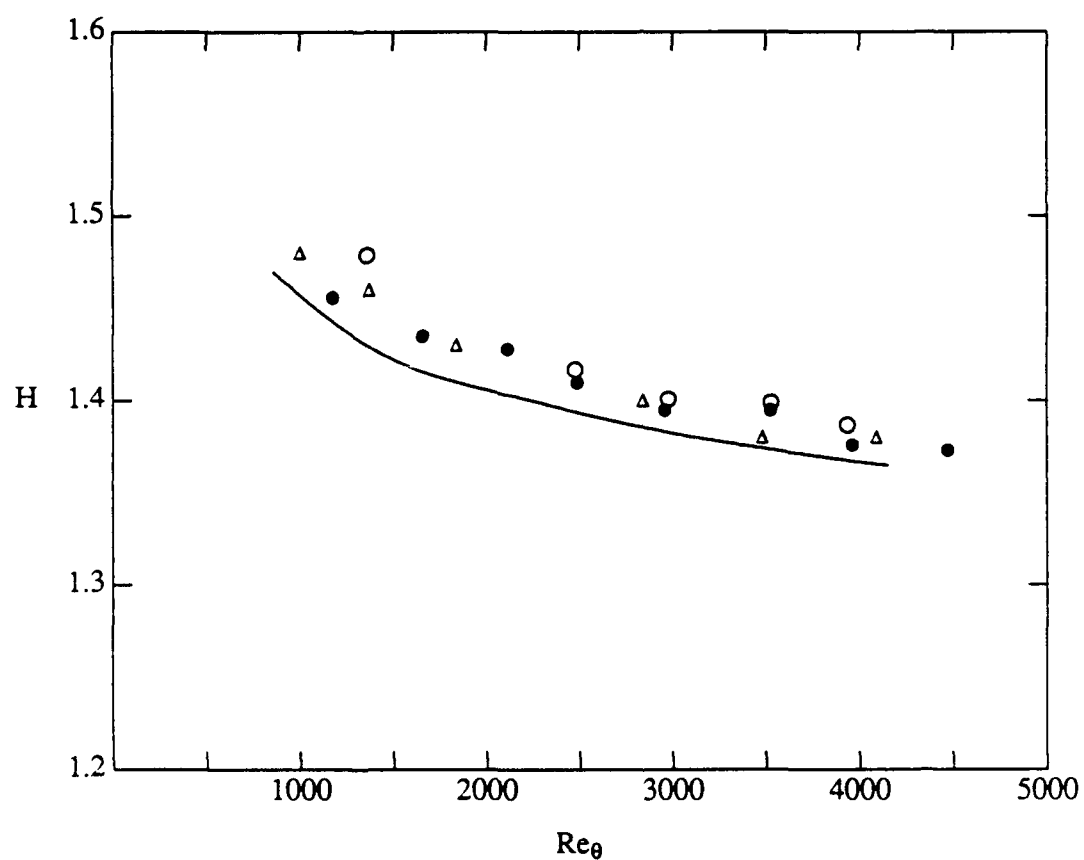
Figure A.1   Variation of shape factor, H, as a function of Re$_\theta$ for a zero pressure gradient
Newtonian boundary layer: o present data; ∆ Purtell et al. (1981); ● Wieghardt
(Coles re-analysis, 1968); — Coles (1962).
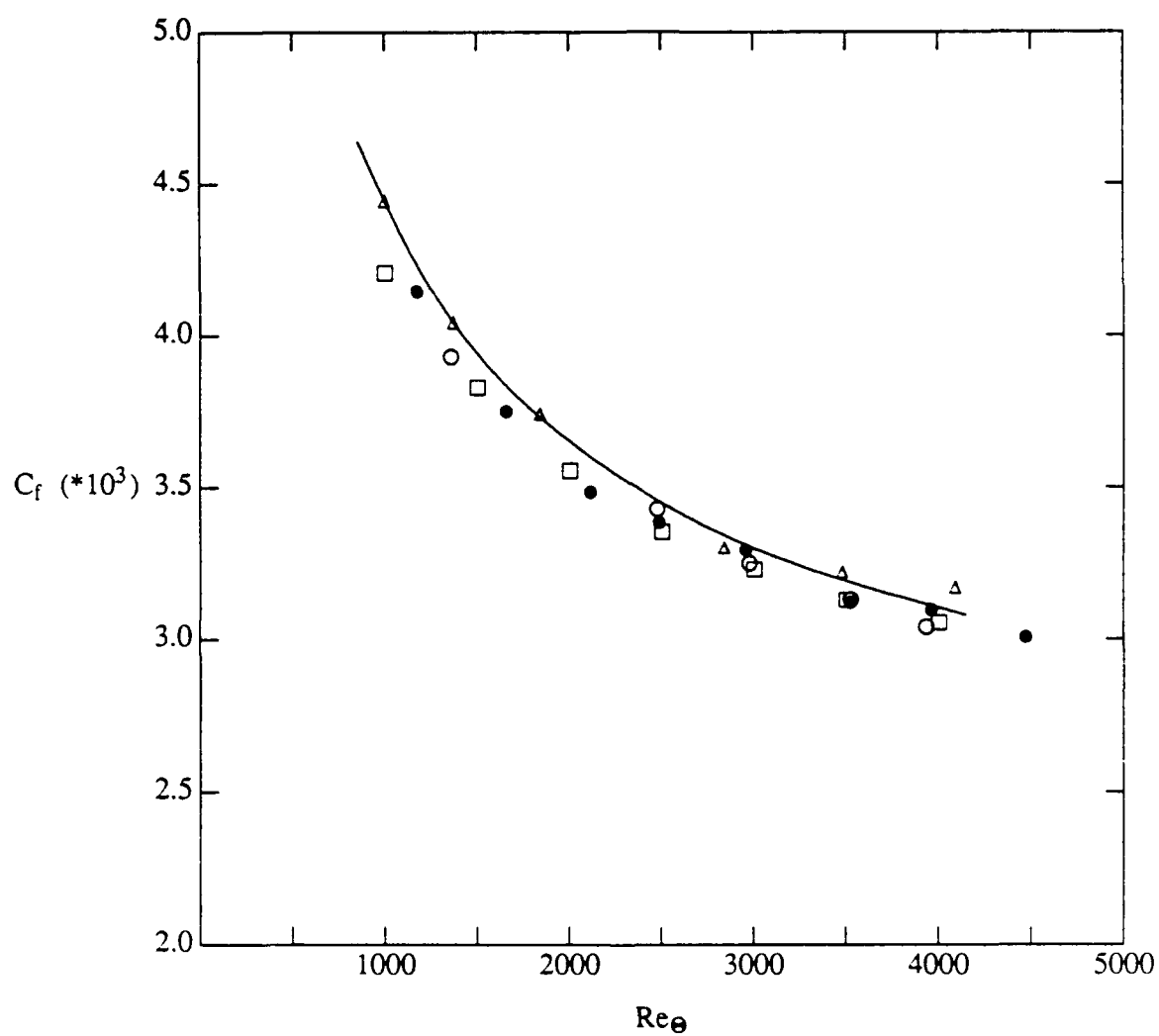
Figure A.2   Variation of skin friction coefficient, C_f, as a function of Re_Θ for a Newtonian zero pressure gradient boundary layer: o present data; ▵ Purtell et. al. (1981); □ Murliss et al. (1982); ● Wieghardt (Coles re-analysis, 1968); — Coles (1962)
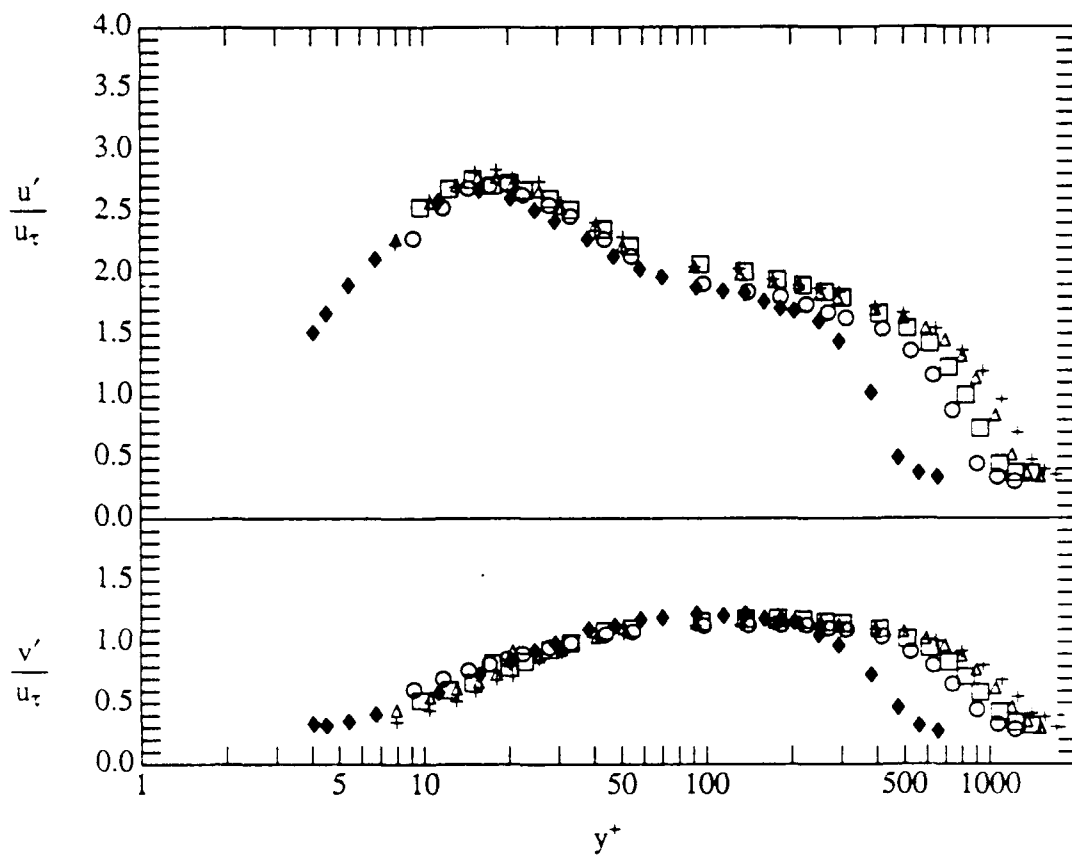
Figure A.3   Root-mean-square rms streamwise and normal velocity fluctuations in a
Newtonian zero pressure gradient boundary layer without injection.
♦ Re_θ =1358; o Re_θ = 2478; □ Re_θ = 2978; ▵ Re_θ = 3527; + Re_θ = 3935.
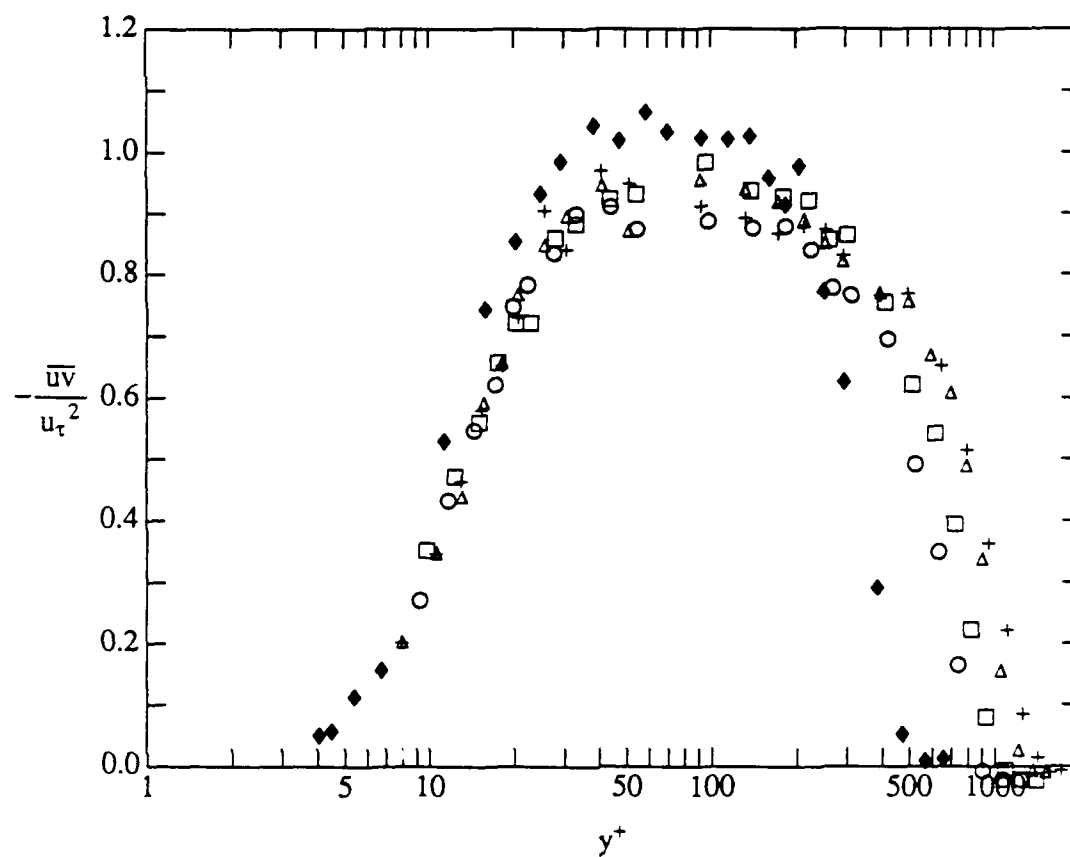
Figure A.4   Reynolds shear stress for a Newtonian zero pressure gradient boundary layer
without injection. ◆ Re_θ =1358; o Re_θ = 2478; □ Re_θ = 2978; ▵ Re_θ = 3527;
+ Re_θ = 3935.
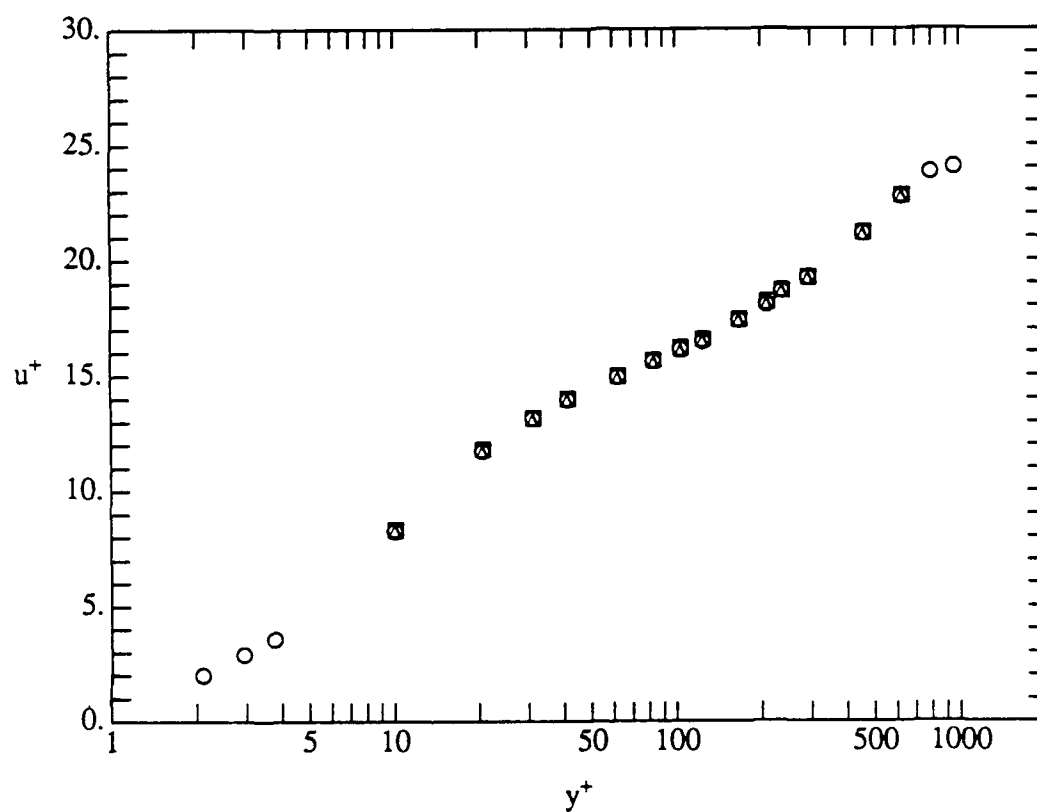
Figure A.5a   Mean streamwise velocity in a Newtonian zero pressure gradient boundary layer
with and without water injection at $Re_\theta = 2495$ o no injection;
□   water injected at $Q_i/Q_s = 1$; ∆   water injected at $Q_i/Q_s = 2$.
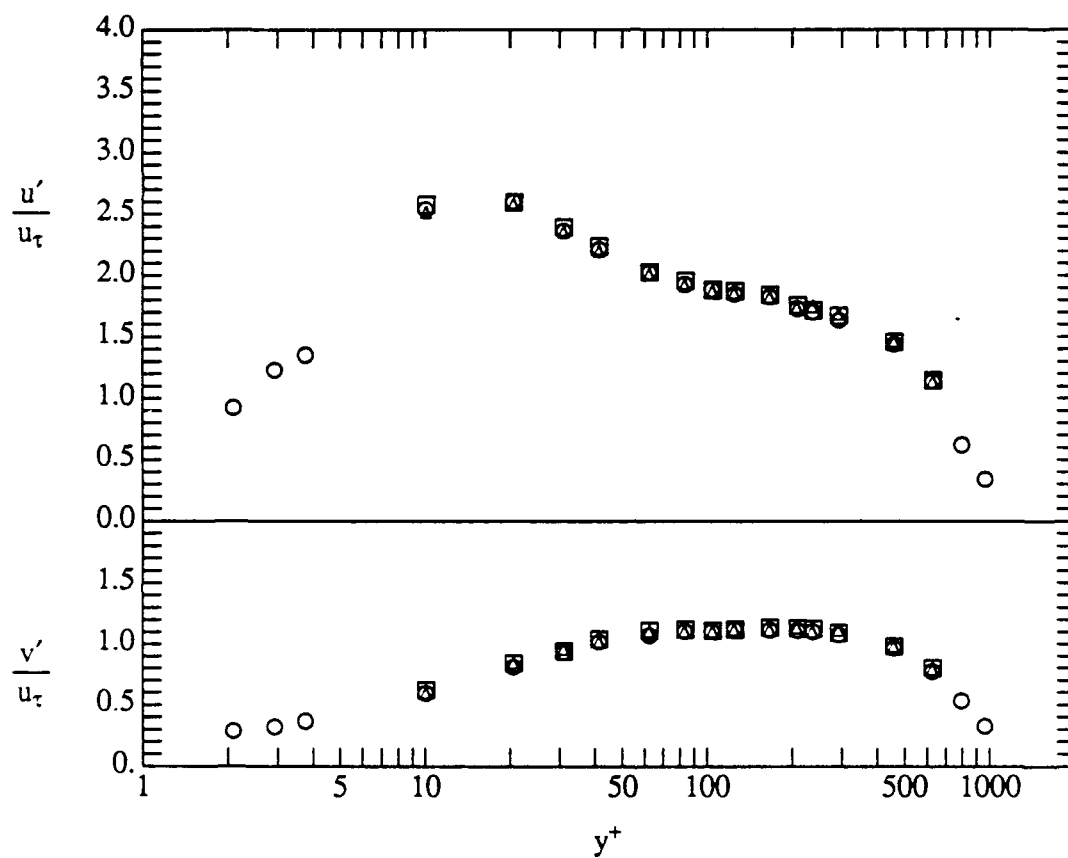
Figure A.5b   Root-mean-square streamwise and normal velocity fluctuations in a Newtonian zero pressure gradient boundary layer with and without water injection at $Re_\theta = 2495$ o no injection; □ water injected at $Q_i/Q_s = 1$; Δ water injected at $Q_i/Q_s = 2$.
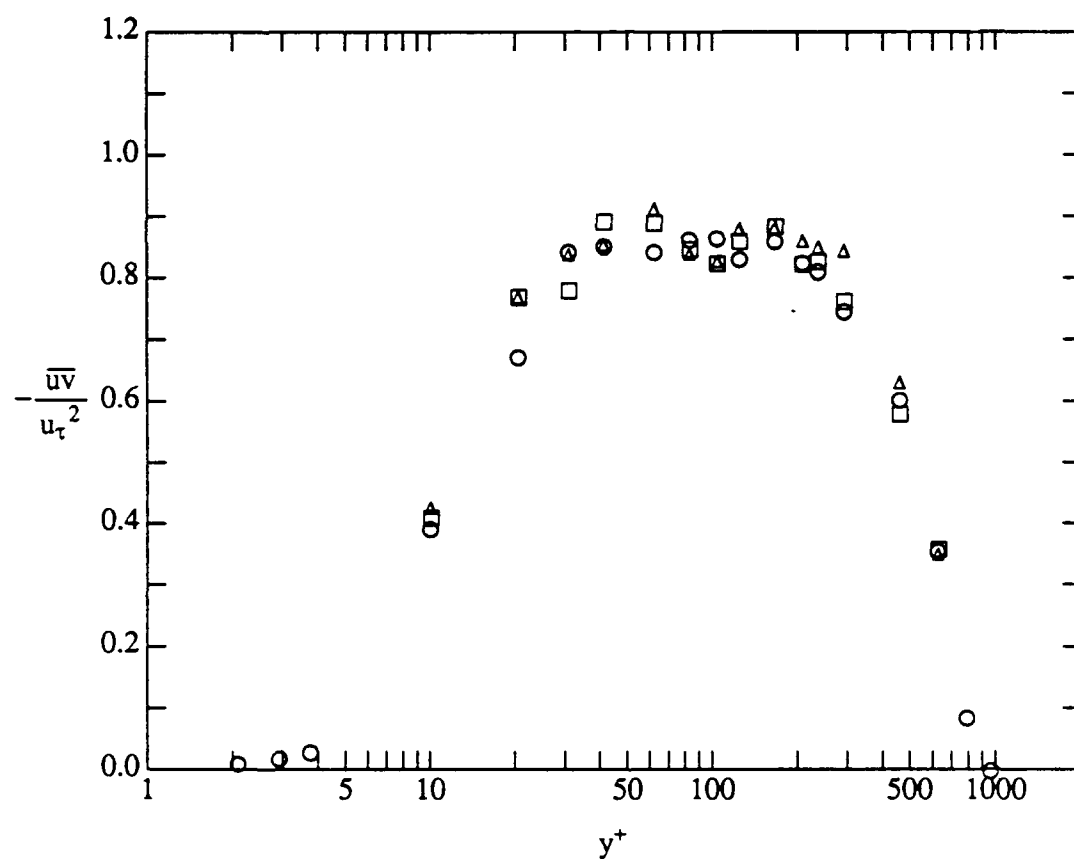
Figure A.5c   Reynolds shear stress in a Newtonian zero pressure gradient boundary layer with
and without water injection at $Re_\theta = 2495$ o no injection;
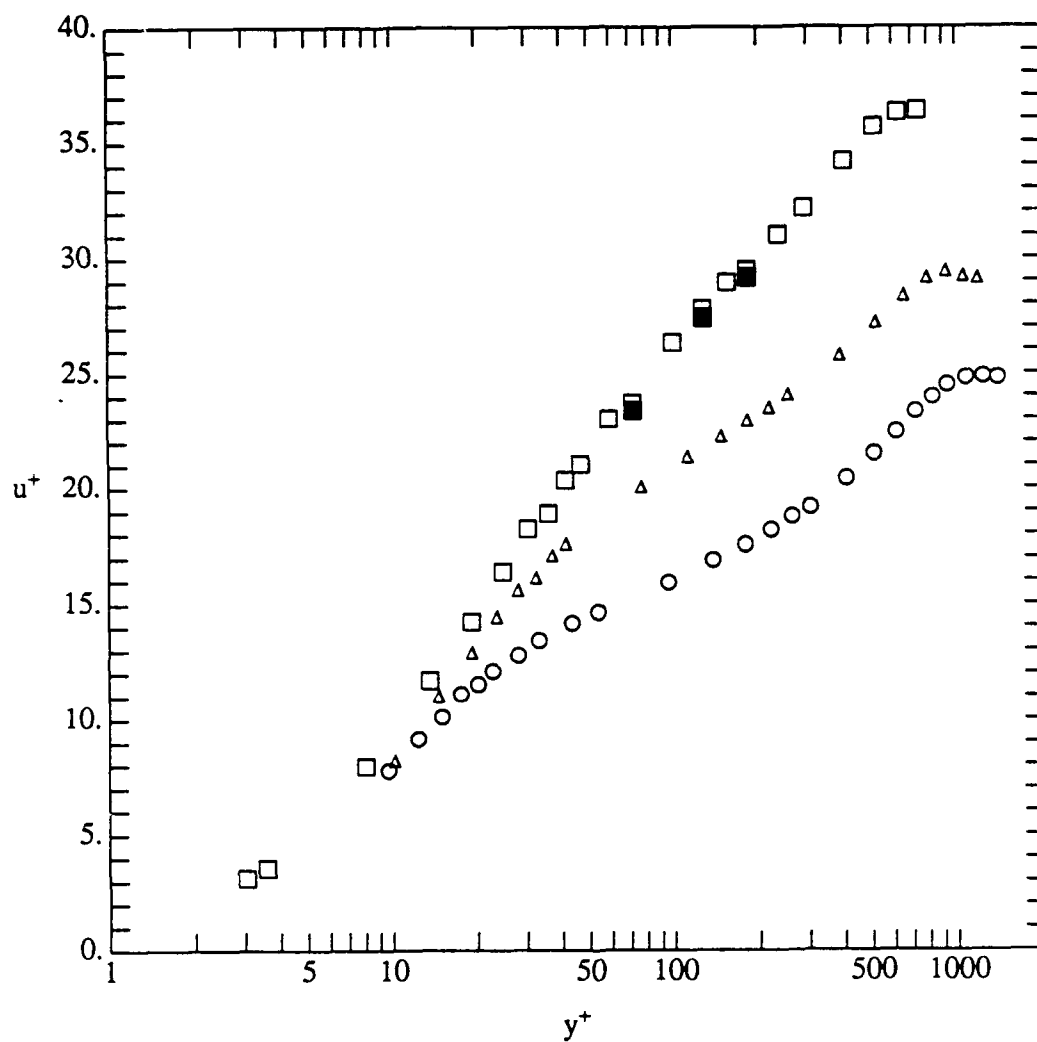□   water injected at $Q_i/Q_s = 1$; △   water injected at $Q_i/Q_s = 2$.
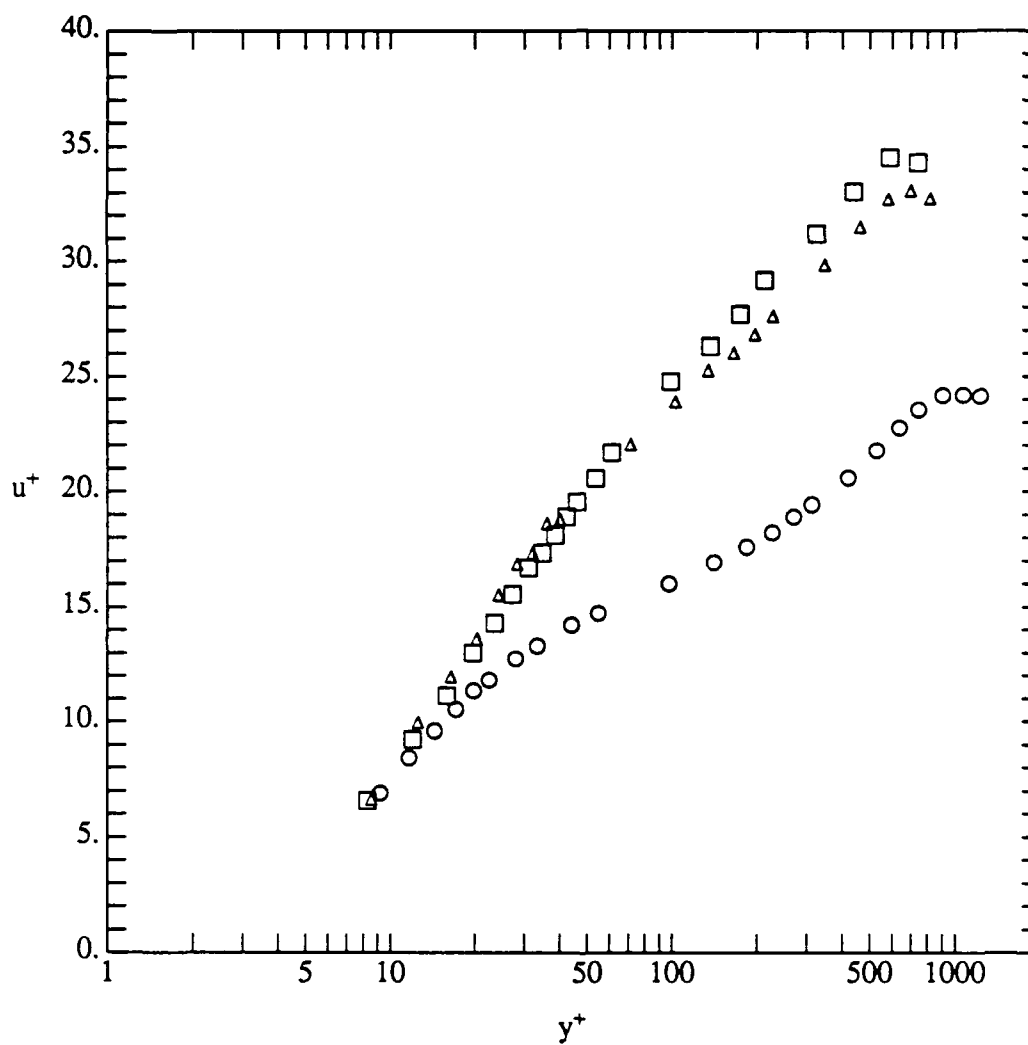
Figure A.6a   Mean streamwise velocity in zero pressure gradient boundary layers comparing drag reduced flows to the Newtonian case at $Re_\theta |_N = 2478$, $x/\delta_s = 52$, $x^+ = 29000$
o $Q_i/Q_s = 0$; $\triangle$ $Q_i/Q_s = 1$; $\square$ $Q_i/Q_s = 2$.
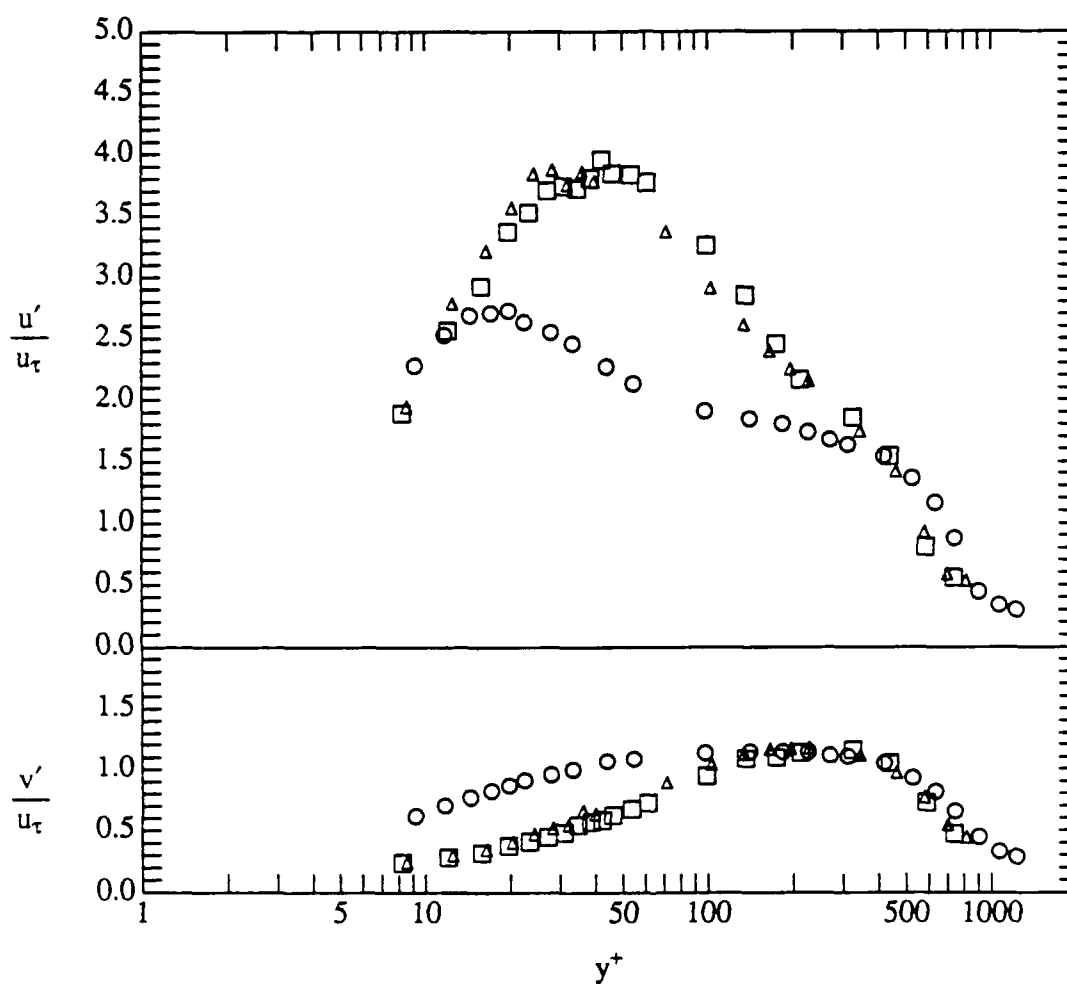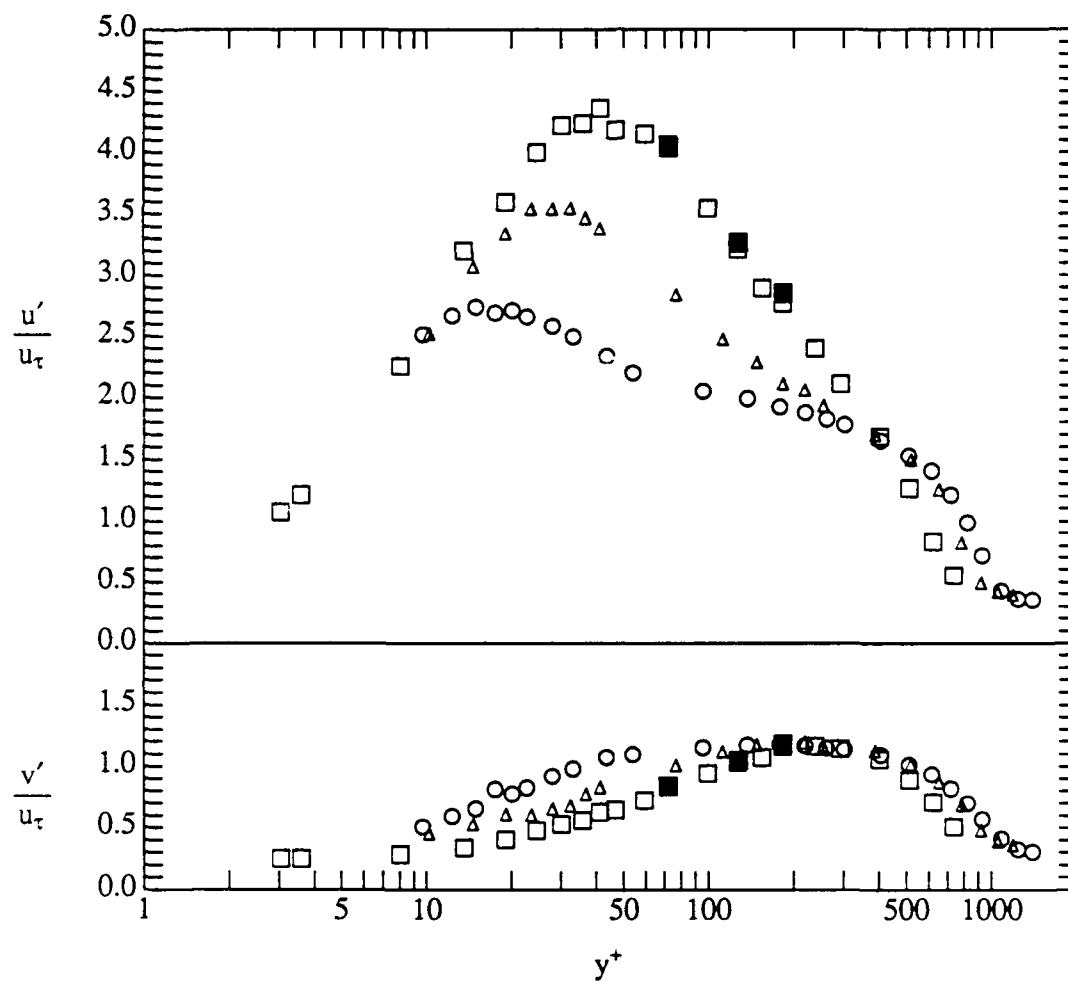
Figure A.6b   Root-mean-square streamwise and normal velocity fluctuations in zero pressure
gradient boundary layers comparing drag reduced flows to the Newtonian case at
$Re_\theta |_N = 2478$, $x/\delta_s = 52$, $x^+ = 29000$ o $Q_i/Q_s = 0$; ∆ $Q_i/Q_s = 1$; □ $Q_i/Q_s = 2$.
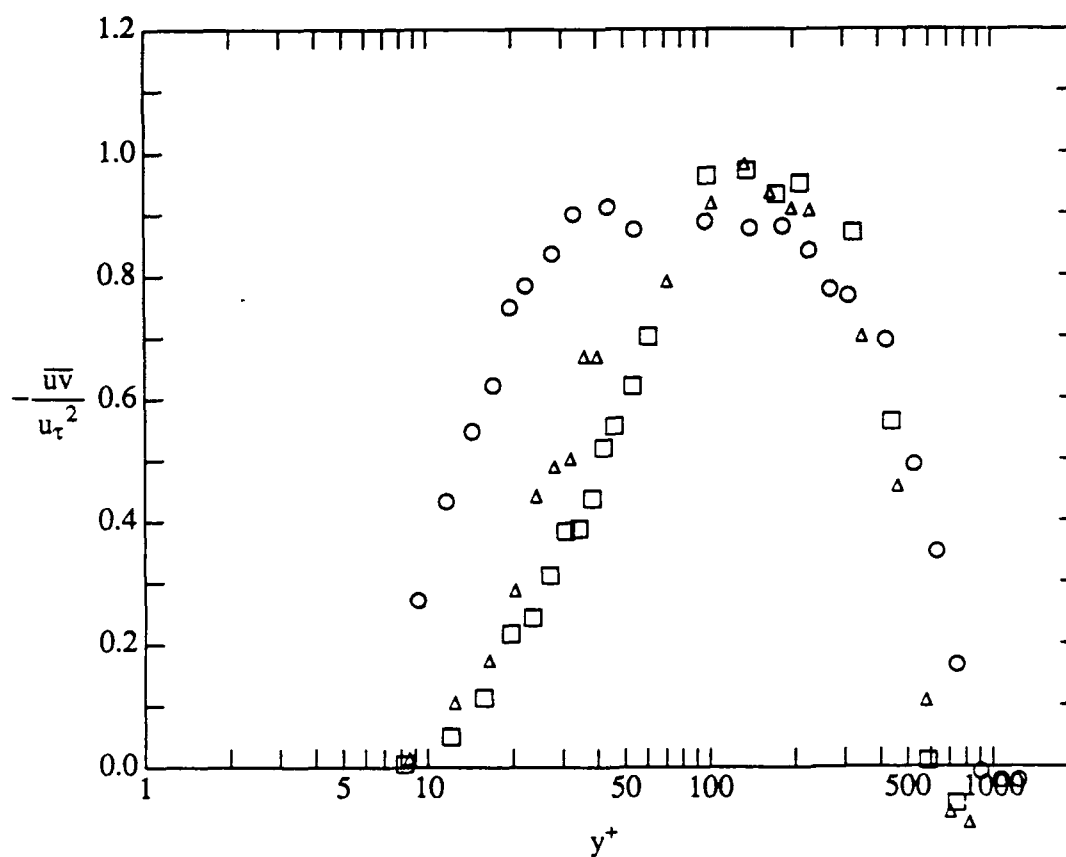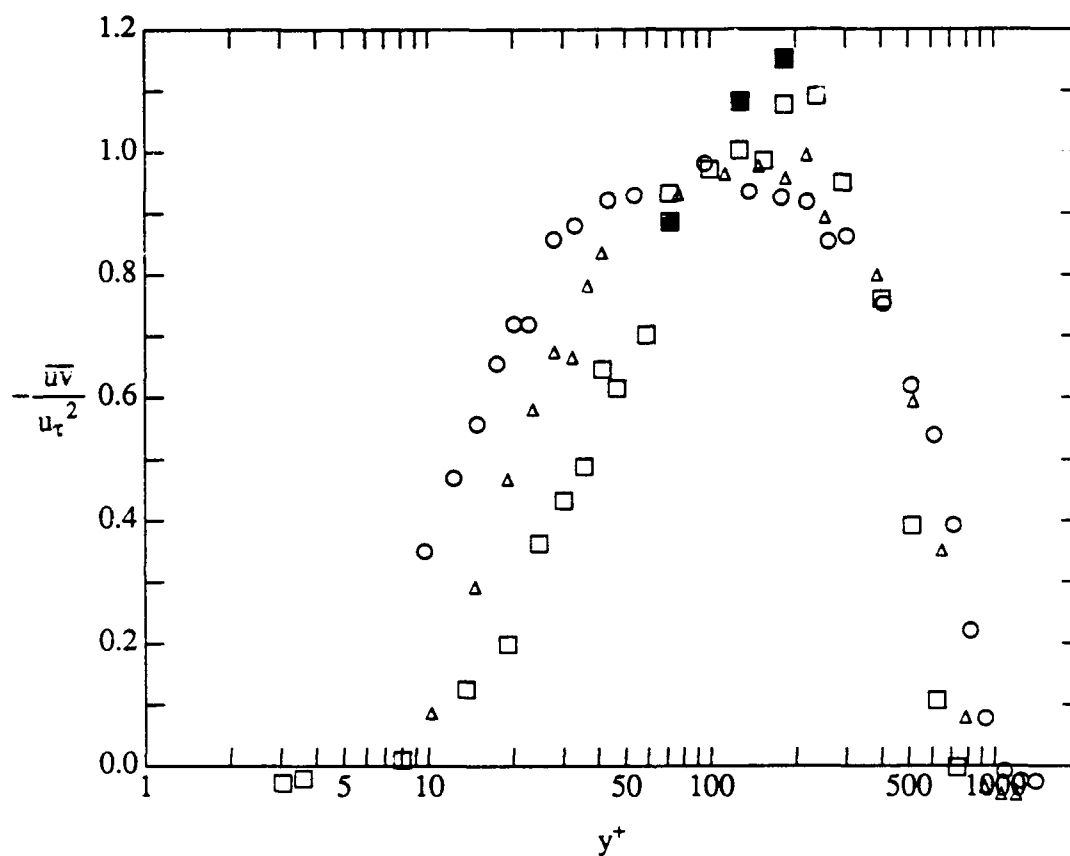
Figure A.6c   Reynolds shear stress in zero pressure gradient boundary layers comparing drag
reduced flows to the Newtonian case at $Re_\theta |_N = 2478$, $x/\delta_s = 52$, $x^* = 29000$

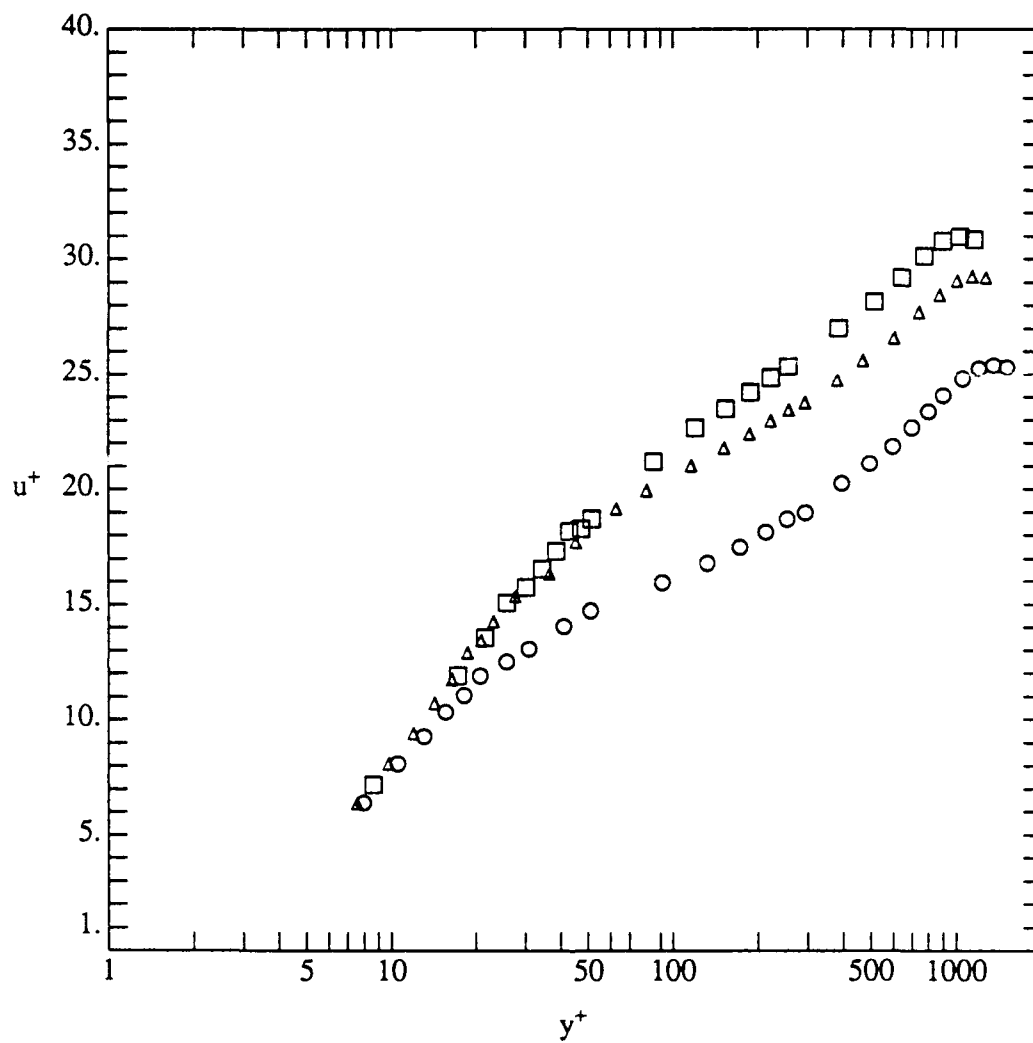o $Q_i/Q_s = 0$; $\triangle$ $Q_i/Q_s = 1$; $\square$ $Q_i/Q_s = 2$.

Figure A.7a   Mean streamwise velocity in zero pressure gradient boundary layers comparing drag reduced flows to the Newtonian case at $Re_\theta|_N = 2978$, $x/\delta_s = 77$, $x^+ = 43200$

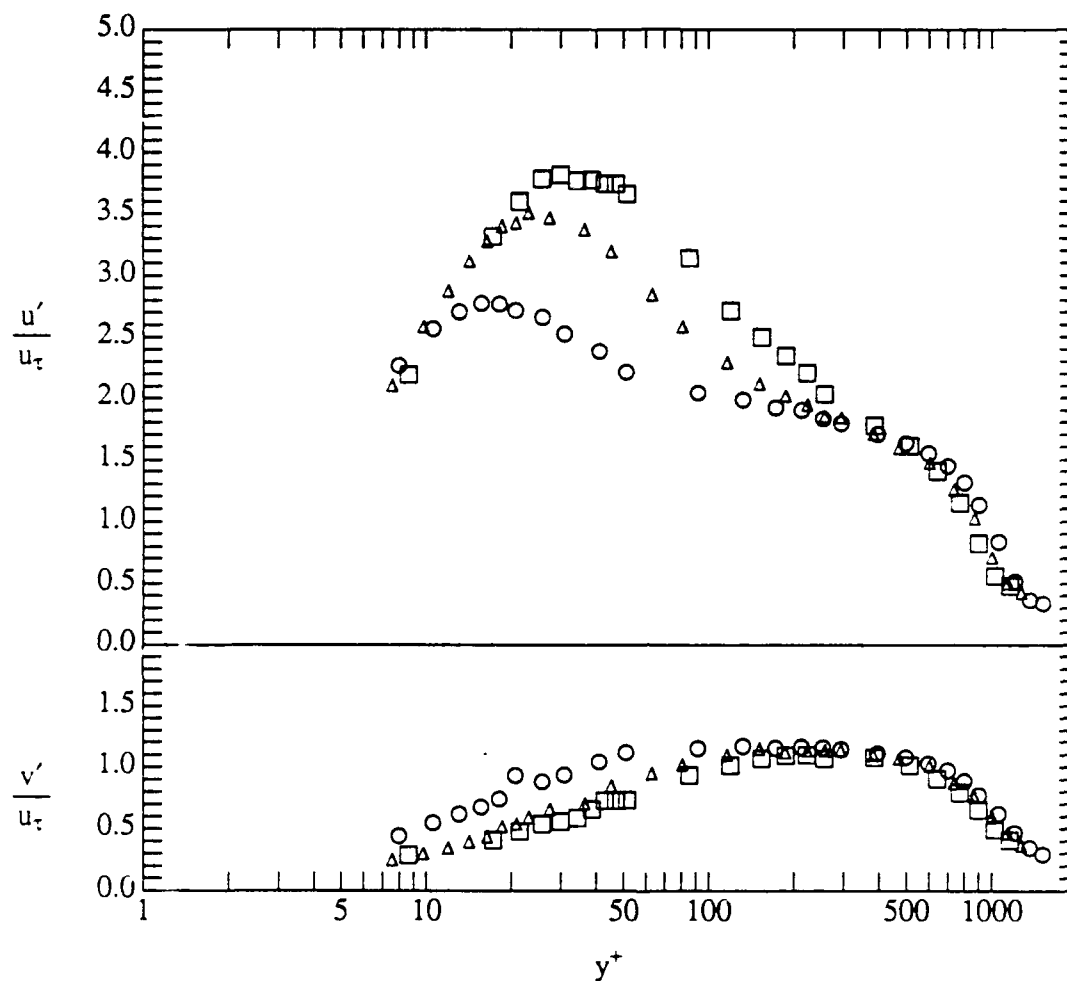o $Q_i/Q_s = 0$; ∆ $Q_i/Q_s = 1$; □ $Q_i/Q_s = 2$; ■ $Q_i/Q_s = 2$ repeated point.

Figure A.7b   Root-mean-square streamwise and normal velocity fluctuations in zero pressure
gradient boundary layers comparing drag reduced flows to the Newtonian case at
$Re_\theta |_N = 2978$, $x/\delta_s = 77$, $x^+ = 43200$ o $Q_i/Q_s = 0$; ▵ $Q_i/Q_s = 1$;
□ $Q_i/Q_s = 2$; ■ $Q_i/Q_s = 2$ repeated point.

Figure A.7c   Reynolds shear stress in zero pressure gradient boundary layers comparing drag
reduced flows to the Newtonian case at $Re_\theta |_N = 2978$, $x/\delta_s = 77$, $x^+ = 43200$

   o $Q_i/Q_s = 0$; ∆ $Q_i/Q_s = 1$;

   □ $Q_i/Q_s = 2$; ■ $Q_i/Q_s = 2$ repeated point.

Figure A.8a. Mean streamwise velocity in zero pressure gradient boundary layers comparing
drag reduced flows to the Newtonian case at
$Re_\theta|_N = 3527$, $x/\delta_s = 115$, $x^+ = 64400$ o $Q_i/Q_s = 0$; Δ $Q_i/Q_s = 1$; $\square$ $Q_i/Q_s = 2$.

Figure A.8b   Root-mean-square streamwise and normal velocity fluctuations in zero pressure gradient boundary layers comparing drag reduced flows to the Newtonian case at $Re_\theta \mid_N = 3527$ $x/\delta_s = 115$ $x^* = 64400$ o $Q_i/Q_s = 0$; $\triangle$ $Q_i/Q_s = 1$; $\square$ $Q_i/Q_s = 2$.
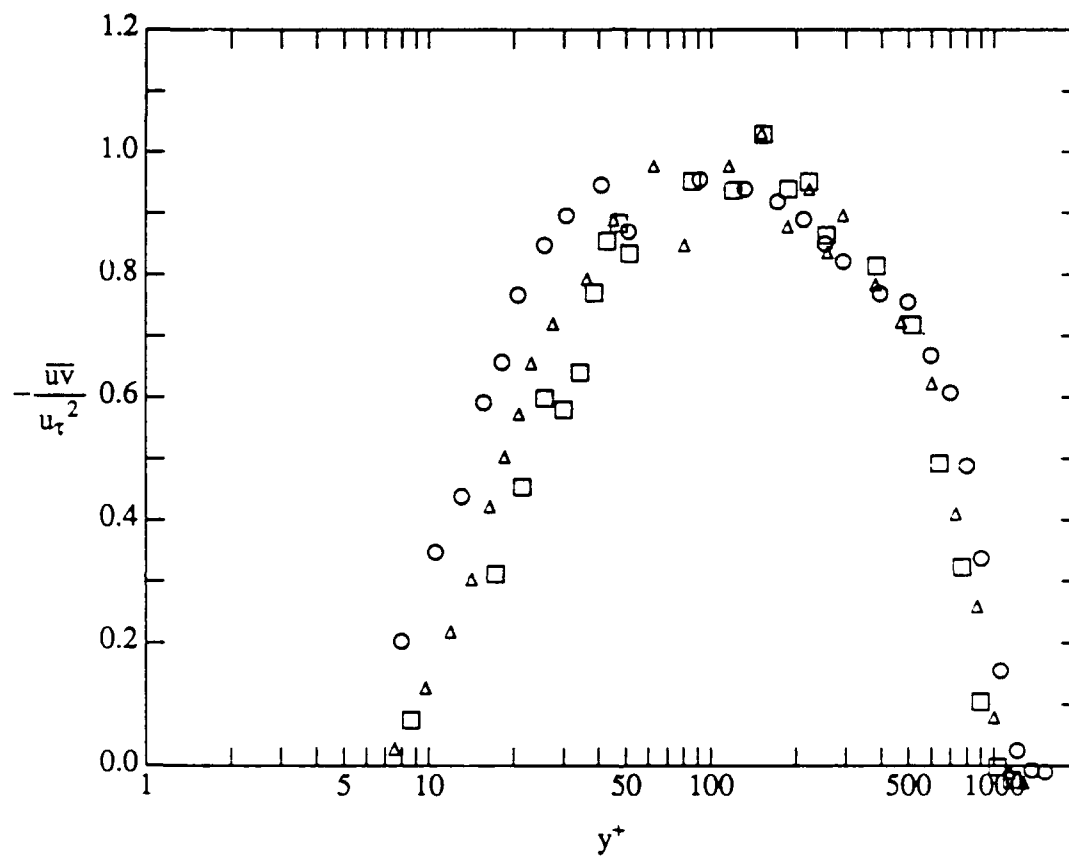
Figure A.8c   Reynolds shear stress in zero pressure gradient boundary layers comparing drag
reduced flows to the Newtonian case at $Re_\theta |_N = 3527$ x/$\delta_s = 115$ x* = 64400
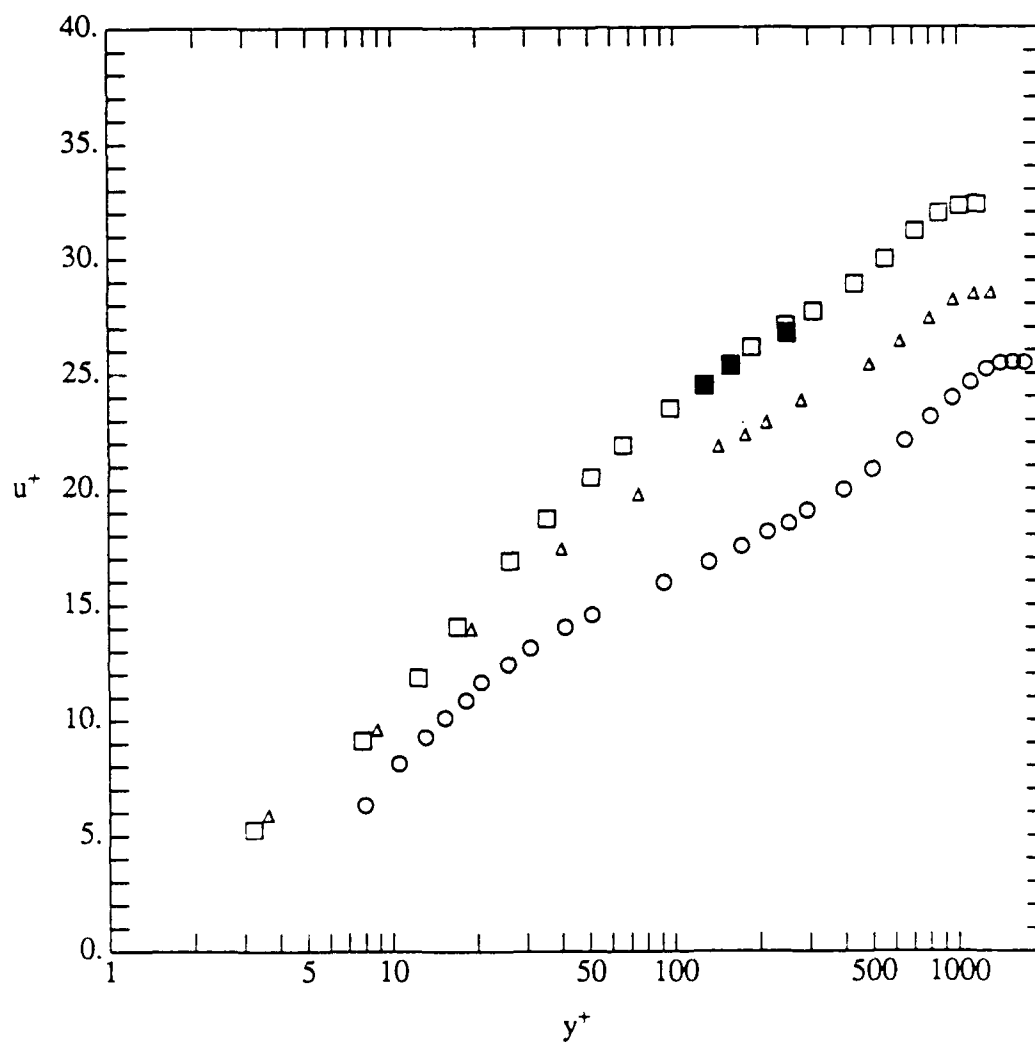o $Q_i/Q_s = 0$; ∆ $Q_i/Q_s = 1$; ☐ $Q_i/Q_s = 2$.

Figure A.9a   Mean streamwise velocity in zero pressure gradient boundary layers comparing drag reduced flows to the Newtonian case at $Re_\theta |_N = 3935$ $x/\delta_s = 144$ $x^* = 81000$

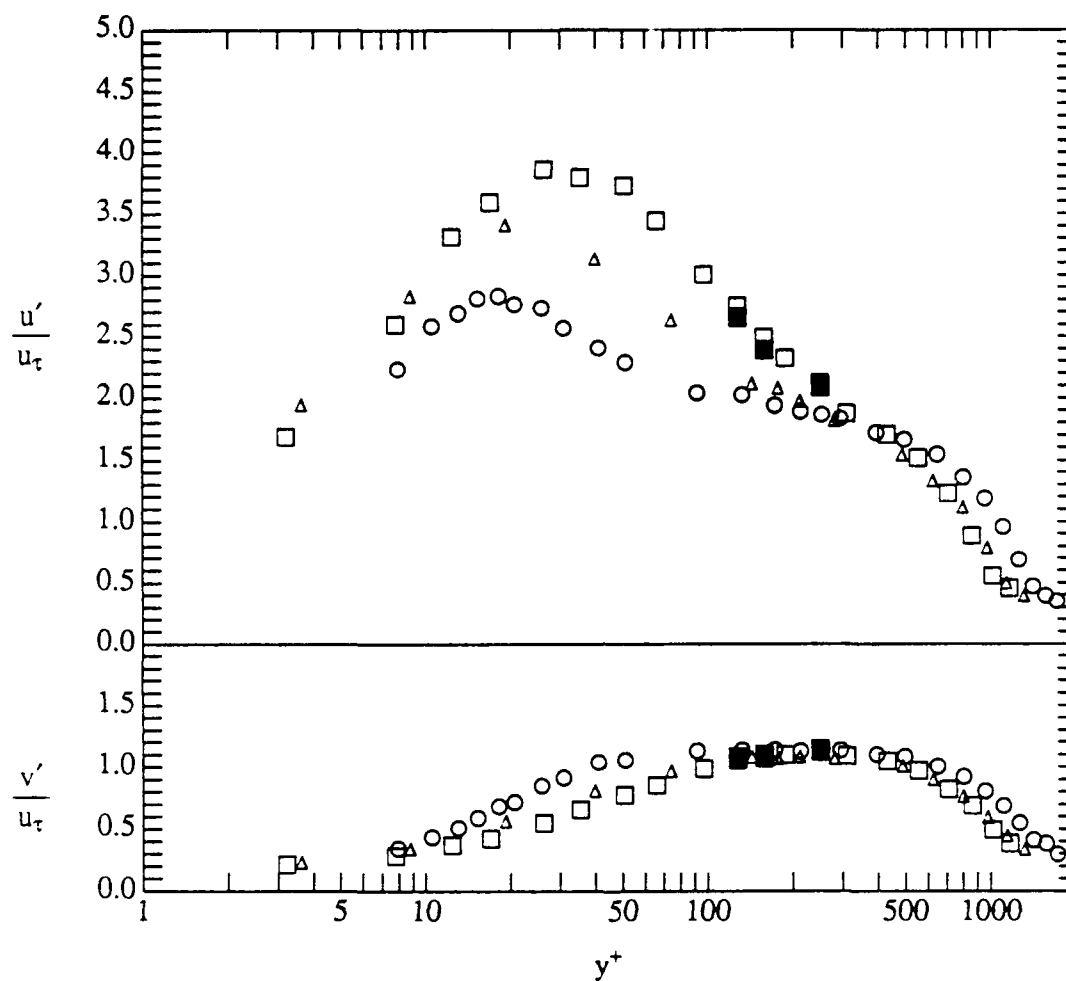o $Q_i/Q_s = 0$; Δ $Q_i/Q_s = 1$; □ $Q_i/Q_s = 2$; ■ $Q_i/Q_s = 2$ repeated points.

Figure A.9b Root-mean-square streamwise and normal velocity fluctuations in zero pressure gradient boundary layers comparing drag reduced flows to the Newtonian case at $Re_\theta |_N = 3935$ $x/\delta_s = 144$ $x^+ = 81000$ o $Q_i/Q_s = 0$; $\triangle$ $Q_i/Q_s = 1$; $\square$ $Q_i/Q_s = 2$; $\blacksquare$ $Q_i/Q_s = 2$ repeated points.
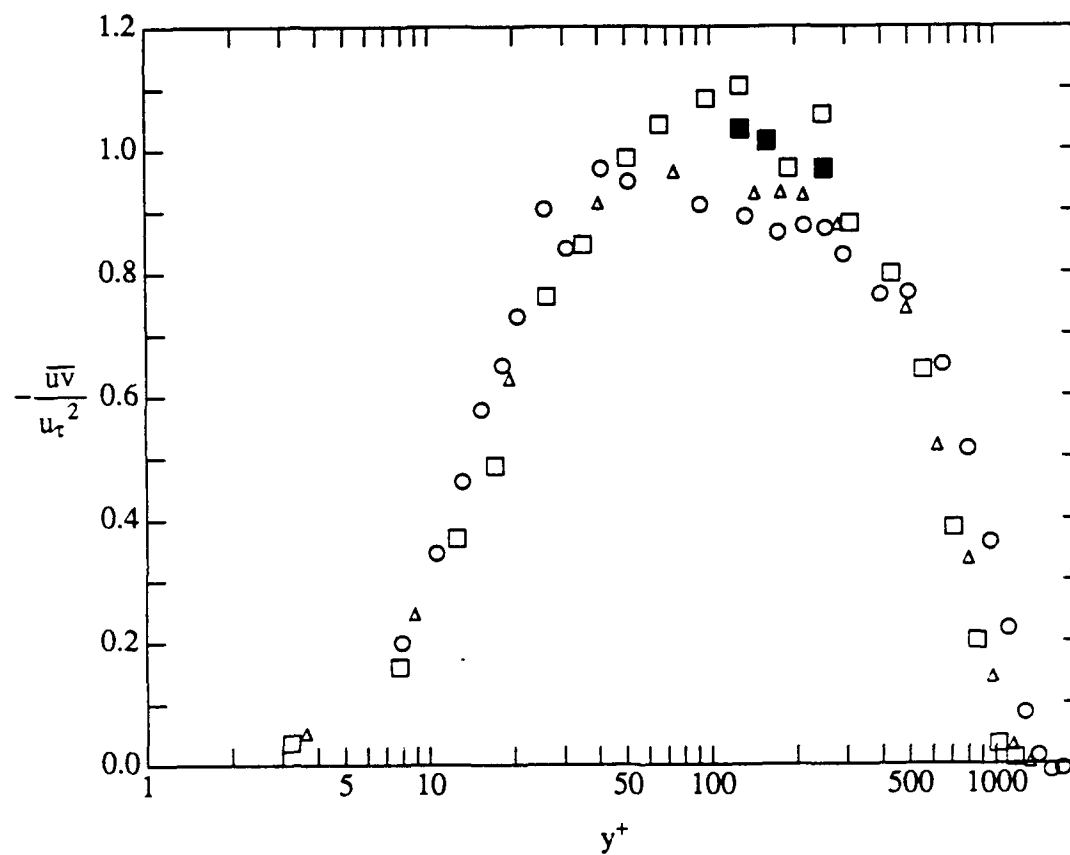
Figure A.9c   Reynolds shear stress in zero pressure gradient boundary layers comparing drag
reduced flows to the Newtonian case at $Re_\theta |_N = 3935$ $x/\delta_s = 144$ $x^* = 81000$

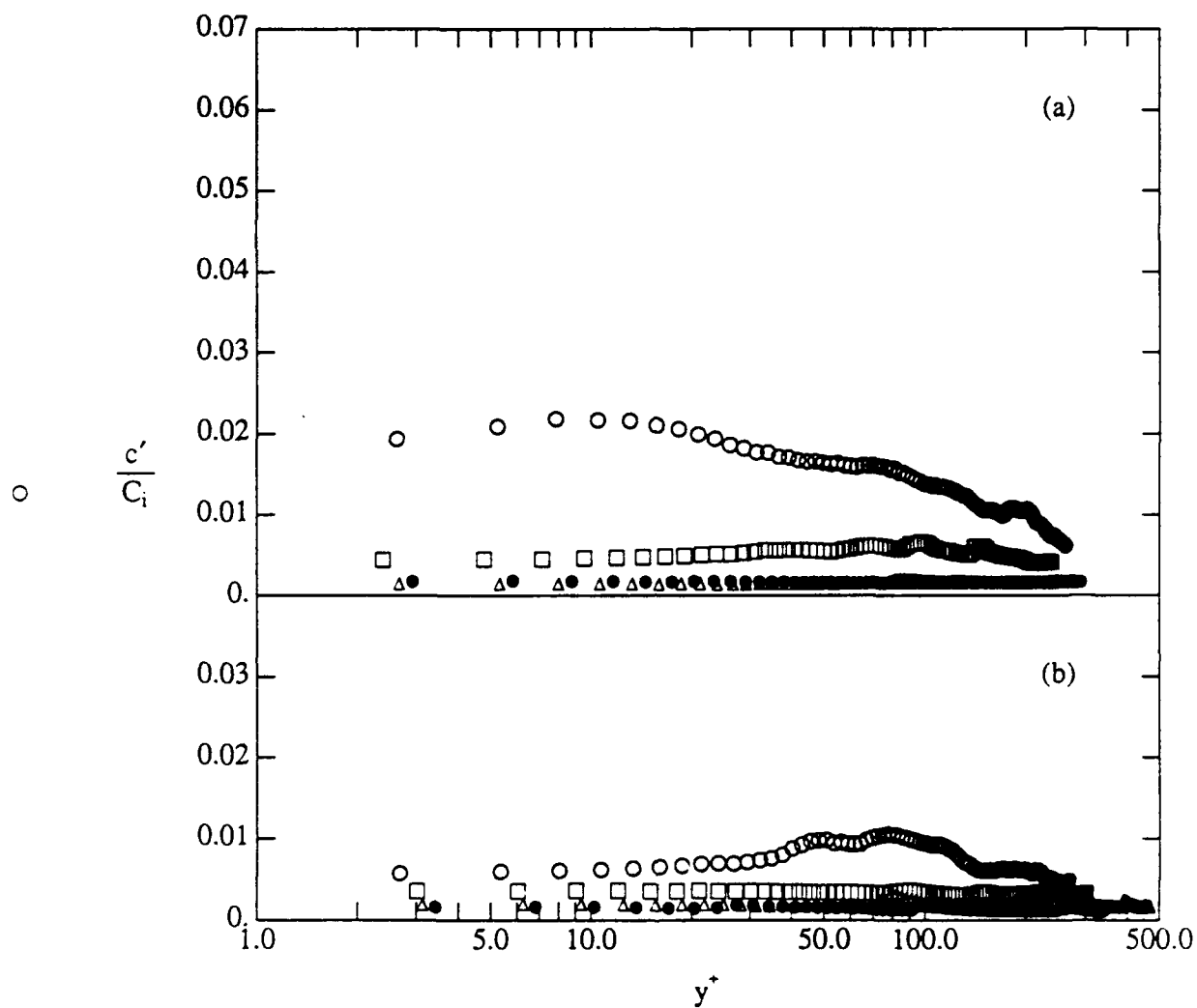○ $Q_i/Q_s = 0$; △ $Q_i/Q_s = 1$; □ $Q_i/Q_s = 2$; ■ $Q_i/Q_s = 2$ repeated points.

Figure A.10 Root-mean-square polymer concentration polymer normalized by the injected
concentration. (a): $Q_i/Q_s = 2$ (b): $Q_i/Q_s = 1$.

    o $Re_\theta |_N = 2478$, $x/\delta_s = 52$, $x^+ = 29000$;

    □ $Re_\theta |_N = 2978$, $x/\delta_s = 77$, $x^+ = 43200$;

    Δ $Re_\theta |_N = 3527$, $x/\delta_s = 115$, $x^+ = 64400$;

    ● $Re_\theta |_N = 3935$, $x/\delta_s = 144$, $x^+ = 81000$.

DISTRIBUTION LIST

Dr. L. Patrick Purtell, Code 1132F
Office of Naval Research
800 North Quincy Street
Arlington, VA 22217-5000

Defense Technical Information Center
Building 5, Cameron Station
Alexandria, VA 22314
(12 copies)

Office of Naval Research
Resident Representative
536 Clark Street, Rm. 286
Chicago, IL 60605-1588

Mechanical Engineering Business Office
Purdue University
West Lafayette, IN 47907

Greg Anderson
Code 634
Naval Ocean System Center
San Diego, CA 92152

Dr. R.J. Hansen
Code 1215
Office of Naval Research
800 North Quincy Street
Arlington, VA 22217

Prof. R.F. Blackwelder
University of Southern California
Dept. of Aerospace Engineering
University Park
Los Angeles, CA 90089-1191

Dr. J.H. Haritonidis
Dept. of Aeronautical & Astronautical Engr.
Ohio State University
Columbus, OH 43210

Prof. D.G. Bogard
Department of Mechanical Engineering
The University of Texas
Austin, TX 78712

Eric W. Hendricks
Code 634
Naval Ocean System Center
San Diego, CA 92152

Dr. Steve Deutsche
ARL
Pennsylvania State University
P.O. Box 30
State College, PA 16801

Mr. G.W. Jones
DARPA/NTO
1515 Wilson Blvd.
Arlington, VA 22209

Prof. T.J. Hanratty
Dept. of Chemical Engineering
1209 West California Street
Box C-3
Urbana, IL 61801

Dr. John Kim
M.S. 202A-1
NASA-Ames Research Center
Moffett Field, CA 94035

Dr. O. Kim
Code 6124
Naval Research Laboratory
Washington, DC 20375

Prof. S.J. Kline
Thermosciences Division
Dept. of Mechanical Engineering
Stanford University
Stanford, CA 94305

G. Leal
Dept. of Chemical & Nuclear Engineering
University of California
Santa Barbara, CA 93106

Justin H. McCarthy
Code 1540
David Taylor Research Center
Bethesda, MD 20084

Dr. C.L. Merkle
Dept. of Mechanical Engineering
Pennsylvania State University
State College, PA 16801

Richard H. Nadolink
Code 821
Naval Underwater Systems Center
Bldg. 679/1
Newport, RI 02841-5047

Steve Robinson
M.S. 163
NASA-Langley Research Center
Hampton, VA 23665

W.G. Souders
Code 1543
David Taylor Research Center

Bethesda, MD 20084

J.D. Swearingen
Code 4420
Naval Research Laboratory
Washington, DC 20375

Prof. David T. Walker
Dept. of Naval Archtechture
and Marine Engineering
North Campus
Ann Arbor, MI 48109-2145

Prof. W.W. Willmarth
Dept. of Aerospace Engineering
University of Michigan
Ann Arbor, MI 48109